7838 *Inorg. Chem.* **2009**, *48*, 7838–7852
DOI: 10.1021/ic900814b

Inorganic Chemistry
Article

Prediction of the Spin Transition Temperature in Fe^{II} One-Dimensional Coordination Polymers: an Anion Based Database

Marinela M. Dîrtu,[†] Aurelian Rotaru,[‡,§] Damien Gillard,[†] Jorge Linares,[‡] Epiphane Codjovi,[‡] Bernard Tinant,[∥] and Yann Garcia*[,†]

[†]*Unité de Chimie des Matériaux Inorganiques et Organiques, Département de Chimie, Université Catholique de Louvain, Place L. Pasteur 1, 1348 Louvain-la-Neuve, Belgium,* [‡]*Groupe d'Etude de la Matière Condensée, 45 avenue des Etats-Unis, Université de Versailles Saint Quentin en Yvelines, 78035 Versailles Cedex, France,* [§]*Department of Solid State and Theoretical Physics, "Alexandru Ioan Cuza" University, 700506 Iasi, Romania, and* [∥]*Unité de Chimie Structurale et des Mécanismes Réactionnels, Département de Chimie, Université Catholique de Louvain, Place L. Pasteur 1, 1348 Louvain-la-Neuve, Belgium*

Received April 27, 2009

One-dimensional (1D) coordination polymers of formula $[Fe(NH_2trz)_3]A\cdot nH_2O$, {A = TiF_6^{2-}, n = 0.5 (**1**) and n = 1 (**2**); A = ZrF_6^{2-}, n = 0.5 (**3**) and n = 0 (**4**); A = SnF_6^{2-}, n = 0.5 (**5**) and n = 1 (**6**); A = TaF_7^{2-}, n = 3 (**7**) and n = 2.5 (**8**); A = GeF_6^{2-}, n = 1 (**9**) and n = 0.5 (**10**), NH_2trz = 4-amino-1,2,4-triazole} have been synthesized, fully characterized, and their spin crossover behavior carefully studied by SQUID magnetometry, Mössbauer spectroscopy, and differential scanning calorimetry. These materials display an abrupt and hysteretic spin transition around 200 K on cooling, as well as a reversible thermochromic effect. Accurate spin transition curves were derived by ^{57}Fe Mössbauer spectroscopy considering the corrected f factors for the high-spin and low-spin states determined employing the Debye model. The unusual hysteresis width of **3** (28 K), was attributed to a dense hydrogen bonding network involving the ZrF_6^{2-} counteranion and the 1D chains, an organization which is also revealed in $[Cu(NH_2trz)_3]ZrF_6\cdot H_2O$ (**11**). Trinuclear spin crossover compounds of formula $[Fe_3(NH_2trz)_{10}(H_2O)_2](SbF_6)_6\cdot S$ {S = 1.5CH_3OH (**12**), 0.5C_2H_5OH (**13**)} were also obtained. A structural property relationship was derived between the volume of the inserted counteranion and the transition temperature $T_{1/2}$ of the 1D chains. Two linear size regimes were identified for monovalent anions ($0.04 \leq V$ (nm^3) ≤ 0.09) and for divalent anions (above $V \geq 0.11$ nm^3) with saturation around $T_{1/2}$ = 200 K. These characteristics allowed us to derive an anion based database that is of interest for the prediction of the transition temperature of such functional switchable materials. Diffuse reflectivity measurements under hydrostatic pressure for **3**,**4** combined with calorimetric data allow an estimation of the electrostatic pressure between cationic chains and counteranions in the crystal lattice of these materials. The chain length distribution that ranges between 1 and 4 nm was also derived.

1. Introduction

Major developments in advanced electronic technology require new switchable magnetic materials presenting a bistability behavior around room temperature. Iron(II) spin transition (ST) coordination compounds belong to such an appealing class of switchable materials with spin state being reversibly triggered by temperature, pressure, or electromagnetic radiation.[1] In this context, the reversible thermochromic ST of one-dimensional (1D) chain compounds of formula $[Fe(NH_2trz)_3](anion)_2\cdot nH_2O$ (NH_2trz = 4-amino-1,2,4-triazole), that can occur around room temperature, has been thoroughly investigated,[2,3] with prospective potential

*To whom correspondence should be addressed. E-mail: yann.garcia@uclouvain.be. Fax: +32-10-472330.

(1) (a) Gütlich, P.; Hauser, A.; Spiering, H. *Angew. Chem.* **1994**, *106*, 2109. Gütlich, P.; Hauser, A.; Spiering, H. *Angew. Chem., Int. Ed. Engl.* **1994**, *33*, 2024. (b) Gütlich, P.; Hauser, A.; Spiering H. In *Inorganic Electronic Structure and Spectroscopy, Vol. II*; A. B. Lever, P., Solomon E. I., Eds.; John Wiley & Sons: New York, 1999 p 575. (c) Gütlich, P.; Garcia, Y.; Goodwin, H. A. *Chem. Soc. Rev.* **2000**, *29*, 419. (d) Gütlich, P.; Garcia, Y.; Woike, Th. *Coord. Chem. Rev.* **2001**, *219−221*, 839. (e) Gütlich, P.; Garcia, Y.; Spiering, H. In *Magnetism: From Molecules to Materials, Vol. IV*; Miller, J. S., Drillon, M., Eds.; Wiley-VCH, New York, 2003; p 271. (f) Spin Crossover in Transition Metal Compounds. In *Top. Curr. Chem.*; Gütlich, P.; Goodwin, H. A., Eds.; Springer: Berlin-Heidelberg, 2004; Vols. *233−235*.

(2) (a) Lavrenova, L. G.; Ikorskii, V. N.; Varnek, V. A.; Oglezneva, I. M.; Larionova, S. V. *Koord. Khim.* **1986**, *12*, 207. (b) Lavrenova, L. G.; Ikorskii, V. N.; Varnek, V. A.; Oglezneva, I. M.; Larionov, S. V. *Koord. Khim.* **1990**, *16*, 654. (c) Lavrenova, L. G.; Yudina, N. G.; Ikorskii, V. N.; Varnek, V. A.; Oglezneva, I. M.; Larionov, S. V. *Polyhedron* **1995**, *14*, 1333. (d) Lavrenova, L. G.; Shakirova, O. G.; Shvedenkov, Y. G.; Ikorskii, V. N.; Varnek, V. A.; Sheludyakova, L. A.; Larionov, S. V. *Koord. Khim.* **1999**, *25*, 208. (e) Lavrenova, L. G.; Shakirova, O. G.; Ikorskii, V. N.; Varnek, V. A.; Sheludyakova, L. A.; Larionov, S. V. *Koord. Khim.* **2003**, *29*, 22.

 Published on Web 07/20/2009

applications (e.g., thermal displays, memory devices, and sensors).[4,5] Because these materials hardly crystallize, their structure was deduced by EXAFS at the Fe−K edge[6−8] and confirmed by single crystal X-ray analyses of a few Cu^{II} analogues.[7f,9−11] It shows linear chains where Fe^{II} ions are bridged by three N_1,N_2-1,2,4-triazoles in the low-spin (LS) state as well as in the high-spin (HS) state.[7] Most of these Fe^{II} complexes exhibit an abrupt ST with hysteresis loops of 2 to 20 K wide that is accompanied by a pronounced thermochromic effect, characteristics which can suit a potential application.[12] The origin of the hysteresis loop was primarily attributed to the effective propagation of short-range elastic cooperative effects through the rigid NH_2trz bridges between neighboring spin changing Fe^{II} ions located at ∼ 3.5 Å each.[7] Indeed, the use of a more flexible bridging ligand connecting the active centers, such as 1,2-bis(tetrazol-1-yl)propane, afforded a linear chain with triply bridged bis monodentate ligands linking the Fe^{II} ions at ∼7 Å. As a result, this compound displays a gradual spin crossover (SCO) behavior on cooling.[13] Decrease of short and long-range elastic cooperative interactions within a polymeric chain were also probed thanks to metal dilution studies of $[Fe_{1-x}M_x(NH_2trz)_3](NO_3)_2$ (M^{II} = Zn, Ni, Mn, Cu),[14] in which a systematic decrease in the steepness of the ST was observed. The intriguing magnetic behavior of the non diluted sample, $[Fe(NH_2trz)_3](NO_3)_2$, that displays a hysteresis loop of 35 K wide[2a,3c] was recently accounted by an extended hydrogen bonding network involving the nitrate anion as part of a three-dimensional (3D) supramolecular lattice of high connectivity involving the 1D chain.[15] This example points out the role of interchain spacing that was not systematically considered in earlier studies.[3] In particular, it is interesting to note that the ST of Fe^{II} 1D chain compounds bearing bulky substituents on the 4-position of the 1,2,4-triazole[16−19] is much less cooperative pointing out at the importance of chain packing in the crystal lattice. It was also noted that the modification of the nature and the geometry of non-coordinated anions can affect the transition temperature, $T_{1/2}$, of these materials without dramatically modifying the hysteresis loop. This feature has been observed for monovalent inorganic anions (Cl^-, Br^-, I^-, BF_4^-, ClO_4^-)[2a−2c] and organic sulfonate anions (alkyl,[3a,3f,3h] phenyl derivatives,[3c,3e,3g] 2-naphthalene derivatives,[3d] and spiropyrane sulfonate[3g]) for the series $[Fe(NH_2trz)_3](anion)_2\cdot nH_2O$. Indeed, the insertion of spherical counteranions, such as halogen anions, leads to higher $T_{1/2}$ as compared with bulkier anions such as BF_4^- and ClO_4^-. A relationship was proposed between the anion radii and the transition temperatures for $[Fe(hyetrz)_3]A_2\cdot nH_2O$ (hyetrz = 4-(2′-hydroxyethyl)-1,2,4-triazole ; A = Cl^-, NO_3^-, Br^-, I^-, BF_4^-, ClO_4^-, PF_6^-),[20] but little is known, however, on the role of divalent anions in promoting/decreasing interchain interactions in such 1D switchable systems. We selected in this work novel fluorinated inorganic anions (TiF_6^{2-}, ZrF_6^{2-}, SnF_6^{2-}, GeF_6^{2-}, TaF_7^{2-}) that are expected to favor the engineering of H-bonding networks.[21] 1D coordination polymers of formula $[Fe(NH_2trz)_3]Anion\cdot nH_2O$ were thus synthesized, and their ST investigated by a set of relevant techniques. We also report on the crystal structure of $[Cu(NH_2trz)_3]ZrF_6\cdot H_2O$ which represents a rare example of a crystallized 1D chain complex with triple N_1,N_2-1,2,4-triazole bridges. A preliminary account on the ST properties of some of the Fe^{II} materials was communicated.[22]

(3) (a) Drabent, K.; Bronisz, R.; Rudolf, M. F. *Conf. Proc. ICAME95* **1996**, *50*, 7. (b) Bronisz, R.; Drabent, K.; Polomka, P.; Rudolf, M. F. *Conf. Proc. ICAME95* **1996**, *50*, 11. (c) Codjovi, E.; Sommier, L.; Kahn, O. *New. J. Chem.* **1996**, *20*, 503. (d) Van Koningsbruggen, P. J.; Garcia, Y.; Codjovi, E.; Lapouyade, R.; Kahn, O.; Fournès, L.; Rabardel, L. *J. Mater. Chem.* **1997**, *7*, 2069. (e) Toyazaki, S.; Murakami, Y.; Komatsu, T.; Kojima, N.; Yokoyama, T. *Mol. Cryst. Liq. Cryst.* **2000**, *343*, 175. (f) Murakami, Y.; Komatsu, T.; Kojima, N. *Synth. Met.* **1999**, *103*, 2157. (g) Toyazaki, S.; Nakanishi, M.; Komatsu, T.; Kojima, N.; Matsumura, D.; Yokoyama, T. *Synth. Met.* **2001**, *121*, 1794. (h) Kojima, N.; Toyazaki, S.; Itoi, M.; Ono, Y.; Aoki, W.; Kobayashi, Y.; Seto, M.; Yokoyama, T. *Mol. Cryst. Liq. Cryst.* **2002**, *376*, 567.

(4) (a) Kahn, O.; Kröber, J.; Jay, C. *Adv. Mater.* **1992**, *4*, 718. (b) Kahn, O.; Codjovi, E.; Garcia, Y.; Van Koningsbruggen, P. J.; Lapouyade, R.; Sommier, L. In *Molecule-Based Magnetic Materials*; Turnbull, M. M., Sugimoto, T., Thompson, L. K., Eds.; ACS Symposium Series, American Chemical Society: Washington, DC, 1996; Vol. *44*, p 298. (c) Kahn, O.; Jay-Martinez, C. *Science* **1998**, *279*, 44.

(5) Garcia, Y.; Ksenofontov, V.; Gütlich, P. *Hyperfine Interact.* **2002**, *139/140*, 543.

(6) (a) Bausk, N. V.; Erenburg, S. B.; Lavrenova, L. G.; Mazalov, L. N. *J. Struct. Chem.* **1994**, *35*, 509. (b) Erenburg, S. B.; Bausk, N. V.; Lavrenova, L. G.; Mazalov, L. N. *J. Synchr. Rad.* **1999**, *6*, 576. (c) Erenburg, S. B.; Bausk, N. V.; Lavrenova, L. G.; Mazalov, L. N. *J. Magn. Magn. Mater.* **2001**, *226*, 1967.

(7) (a) Michalowicz, A.; Moscovici, J.; Ducourant, B.; Cracco, D.; Kahn, O. *Chem. Mater.* **1995**, *7*, 1833. (b) Michalowicz, A.; Moscovici, J.; Kahn, O. *J. Phys. IV* **1997**, *7*, 633. (c) Garcia, Y.; Van Koningsbruggen, P. J.; Bravic, G.; Guionneau, P.; Chasseau, D.; Cascarano, G. L.; Moscovici, J.; Lambert, K.; Michalowicz, A.; Kahn, O. *Inorg. Chem.* **1997**, *36*, 6357. (d) Michalowicz, A.; Moscovici, J.; Garcia, Y.; Kahn, O. *J. Synchrotron Radiat.* **1999**, *6*, 231. (e) Michalowicz, A.; Moscovici, J.; Charton, J.; Sandid, F.; Benamrane, F.; Garcia, Y. *J. Synchrotron Radiat.* **2001**, *8*, 701. (f) Garcia, Y.; Moscovici, J.; Michalowicz, A.; Ksenofontov, V.; Levchenko, G.; Bravic, G.; Chasseau, D.; Gütlich, P. *Chem.—Eur. J.* **2002**, *8*, 4992.

(8) (a) Yokoyama, T.; Murakami, Y.; Kiguchi, M.; Komatsu, T.; Kojima, N. *Phys. Rev. B* **1998**, *58*, 14238. (b) Kojima, N.; Murakami, Y.; Komatsu, T.; Yokoyama, T. *Synth. Met.* **1999**, *103*, 2154.

(9) Garcia, Y.; Van Koningsbruggen, P. J.; Bravic, G.; Guionneau, P.; Chasseau, D.; Cascarano, G. L.; Moscovici, J.; Lambert, K.; Michalowicz, A.; Kahn, O. *Inorg. Chem.* **1997**, *36*, 6357.

(10) Drabent, K.; Ciunik, Z. *Chem. Commun.* **2001**, 1254.

(11) Garcia, Y.; Van Koningsbruggen, P. J.; Bravic, G.; Chasseau, D.; Kahn, O. *Eur. J. Inorg. Chem.* **2003**, 356.

(12) Garcia, Y.; Niel, V.; Muñoz, M. C.; Real, J. A. *Top. Curr. Chem.* **2004**, *233*, 229.

(13) Van Koningsbruggen, P. J.; Garcia, Y.; Kahn, O.; Fournès, L.; Kooijman, H.; Spek, A. L.; Haasnoot, J. G.; Moscovici, J.; Provost, K.; Michalowicz, A.; Renz, F.; Gütlich, P. *Inorg. Chem.* **2000**, *39*, 1891.

(14) (a) Lavrenova, L. G.; Ikorskii, V. N.; Varnek, V. A.; Oglezneva, I. M.; Larionov, S. V. *J. Struct. Chem.* **1993**, *34*, 960. (b) Shvedenkov, Y. G.; Ikorskii, V. N.; Lavrenova, L. G.; Drebushchak, V. A.; Yudina, N. G. *J. Struct. Chem.* **1997**, *38*, 578. (c) Varnek, A.; Lavrenova, L. G.; Gromikov, S. A. *J. Struct. Chem.* **1997**, *38*, 585. (d) Varnek, V. A.; Lavrenova, L. G. *J. Struct. Chem.* **1997**, *38*, 850. (e) Cantin, C.; Daubric, H.; Kliava, J.; Servant, Y.; Sommier, L.; Kahn, O. *J. Phys.: Condens. Matter* **1998**, *10*, 7057.

(15) Garcia, Y.; Campbell, S. J.; Lord, J. S.; Boland, Y.; Ksenofontov, V.; Gütlich, P. *J. Phys. Chem. B* **2007**, *111*, 11111.

(16) Schwarzenbacher, G.; Gangl, M. S.; Goriup, M.; Winter, M.; Grunert, M.; Renz, F.; Linert, W.; Saf, R. *Monatsh. Chem.* **2001**, *132*, 519.

(17) Fujigaya, T.; Jiang, D. L.; Aida, T. *J. Am. Chem. Soc.* **2005**, *127*, 5484.

(18) (a) Seredyuk, M.; Gaspar, A. B.; Ksenofontov, V.; Reiman, S.; Galyametdinov, Y.; Haase, W.; Rentschler, E.; Gütlich, P. *Hyperfine Interact.* **2006**, *166*, 385. (b) Seredyuk, M.; Gaspar, A. B.; Ksenofontov, V.; Reiman, S.; Galyametdinov, Y.; Haase, W.; Rentschler, E.; Gütlich, P. *Chem. Mater.* **2006**, *18*, 2513.

(19) Sonar, P.; Grunert, C.; Wei, M. Y.−L.; Kusz, J.; Gütlich, P.; Schlüter, A. D. *Eur. J. Inorg. Chem.* **2008**, 1613.

(20) Garcia, Y.; Van Koningsbruggen, P. J.; Lapouyade, R.; Rabardel, L.; Kahn, O.; Wierczorek, M.; Bronisz, R.; Ciunik, Z.; Rudolf, M. F. *C. R. Acad. Sci. Paris* **1998**, *IIc*, 523.

(21) Metrangolo, P.; Meyer, F.; Pilati, T.; Resnati, G.; Terraneo, G. *Angew. Chem., Int. Ed.* **2008**, *47*, 6114.

(22) Dîrtu, M. M.; Garcia, Y.; Nica, M.; Rotaru, A.; Linares, J.; Varret, F. *Polyhedron* **2007**, *26*, 2259.

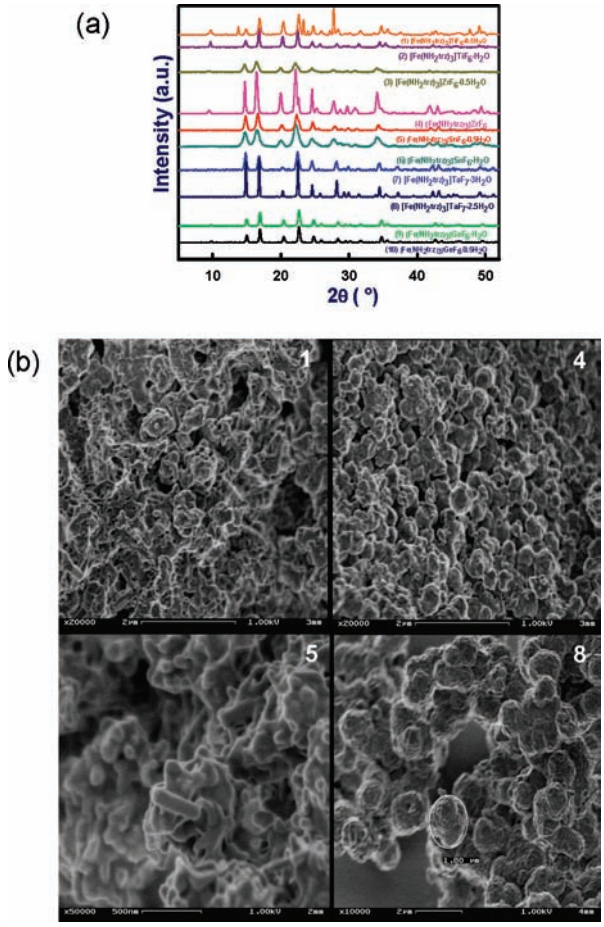

Figure 1. (a) X-ray powder diffraction patterns at 293 K for **1**−**10**. (b) SEM imaging at 293 K for **1**, **4**, **5**, and **8**.

2. Results

2.1. Synthesis. The 1D coordination polymers were obtained as white powders by self-assembly of the corresponding Fe^{II} inorganic precursors $[Fe(H_2O)_6]$Anion, prepared in situ and in air, with an alcoholic solution of NH_2trz (methanol or ethanol). These compounds were successfully characterized by CHN and TGA analyses, atomic absorption, X-ray powder diffraction (293 K), IR, UV−vis, and ^{57}Fe Mössbauer spectroscopy. Thermogravimetric and elemental analyses did not reveal the presence of alcohol guest molecules but instead revealed non-coordinated water molecules, affording the following general formula $[Fe(NH_2trz)_3]$Anion$\cdot n H_2O$: {anion = TiF_6^{2-}, $n = 0.5$ (**1**) and $n = 1$ (**2**); anion = ZrF_6^{2-}, $n = 0.5$ (**3**) and $n = 0$ (**4**); anion = SnF_6^{2-}, $n = 0.5$ (**5**) and $n = 1$ (**6**); anion = TaF_7^{2-}, $n = 3$ (**7**) and $n = 2.5$ (**8**); anion = GeF_6^{2-}, $n = 1$ (**9**) and $n = 0.5$ (**10**)}. Hemihydrate or monohydrate compounds were thus obtained, except for Zr and Ta. Inclusion of solvent used for synthesis was only observed for $[Fe_3(NH_2trz)_{10}(H_2O)_2](SbF_6)_6\cdot S$ {S = $1.5CH_3OH$ (**12**), $0.5C_2H_5OH$ (**13**)} whose trinuclear nature was confirmed by both elemental analysis and Mössbauer spectroscopy (vide infra).

Isostructurality of the chain complexes was concluded from X-ray powder diffraction patterns that revealed the presence of principal peaks in all diffractograms (Figure 1a). Compounds **4** and **8** show the better resolved diffractograms of the series. Spherical particles of 484 nm (**4**) and 1.80 μm (**8**) diameter are distinguished in the aggregates, as well as elongated rods of dimensions (457 × 108 nm) for (**5**) by SEM imaging. Compound **1** is, however, much less crystalline (Figure 1b). This series of materials have also essentially identical IR spectra. The bands assigned to ring torsion of NH_2trz at $\nu = 619$ cm^{-1} and the N−N stretching band at $\nu = 1197$ cm^{-1} are shifted[23] upon complexation to 624 cm^{-1} and 1210 cm^{-1}, respectively, for example, for $[Fe(NH_2trz)_3]ZrF_6$ (**4**). These values confirm a coordination of the iron to the 1,2,4-triazole ring.[24] Presence of non-coordinated divalent counteranions originating from the inorganic precursors is also confirmed by IR as listed in the synthesis section. ^{57}Fe Mössbauer spectroscopy confirms the presence of only one $Fe^{II}N_6$ site, undergoing SCO behavior on cooling and the absence of oxidation product of iron (see Figure 5). Mössbauer parameters of these compounds (see section 2.3.2) are typical for 1D polymeric chains with NH_2trz as ligand.[3d]

These materials including trinuclear complexes, prepared as white powders, present a reversible thermochromism to pink on cooling. These colors depend on the spin state of the Fe^{II} centers. The white color is due to the location of the spin-allowed lowest energy d-d transition, $^5T_{2g} \rightarrow {}^5E_g$, for the HS sites in the near-infrared region ($\sim$11800 cm^{-1}).[2a] The pink color is due to the $^1A_{1g} \rightarrow {}^1T_{1g}$ d-d transition of LS Fe^{II} sites observed at $\sim$19250 cm^{-1}.

2.2. X-ray Crystal Structure of $[Cu(NH_2trz)_3]ZrF_6\cdot H_2O$. Blue needles single crystals of $[Cu(NH_2trz)_3]ZrF_6\cdot H_2O$ (**11**) were successfully obtained by slow evaporation of an aqueous solution of $[Cu(H_2O)_6]ZrF_6$ and NH_2trz at room temperature. Attempts to crystallize other Fe^{II} and Cu^{II} complexes of the series failed. Crystallographic data at 100(1) K and structure refinement of **11** that crystallizes in the monoclinic $P2_1/n$ space group are given in Table 1. Figure 2a shows a view of the 1D polymeric chain built of cationic $[Cu(NH_2trz)_3]^{2+}$ units. The asymmetric unit consists of two Cu^{II} atoms, Cu1 and Cu2, located on inversion centers. These copper ions are linked by three bidentate bridging NH_2trz ligands through *N1*, *N2* atoms. Both copper ions are arranged in a CuN_6 core of octahedral geometry within the chain. The basis of the octahedron is formed by four ligands with bond lengths ranging between 2.014(3)−2.080(3) Å (Table 2). Two NH_2trz ligands are axially coordinated to copper (Cu1−N1 = 2.080(3), Cu2−N12 = 2.385(3) Å) with difference in bond length indicating a distortion. The ligand bridges Cu1 and Cu2 ions almost at the same distance with Cu1−N21 = 2.029(3) Å and Cu2−N22 = 2.029(3) Å. The Cu1−N11 distance is 2.014(3) Å which corresponds to an angle of 122.6(2)° for Cu1−N11−N12. As the distance Cu2−N12 = 2.385(3) Å increases, the (Cu2−N12−N11) angle widens to 125.5(2)°. In this case, only a torsion angle (Cu1−N11−N12−Cu2) = −12.8(3)° maintains this geometry. The coordination mode of *N*1, *N*2 of NH_2trz presents quite a high degree of asymmetry compared to the Cu−N−N bridge angles, which are

(23) Haasnoot, J. G.; Vos, G.; Groeneveld, W. L. *Z. Naturforsch. B* **1977**, *32*, 421.
(24) Sinditskii, V. P.; Sokol, V. I.; Fogel'zang, A. E.; Dutov, M. D.; Serushkin, V. V.; Porai-Koshits, M. A.; Svetlov, B. S. *Russ. J. Inorg. Chem.* **1987**, *32*, 1586.

Table 1. Crystallographic Data and Structure Refinement for $[Cu(NH_2trz)_3]ZrF_6 \cdot H_2O$ (**11**) at 100(1) K[a]

empirical formula	$C_6H_{14}OCuN_{12}ZrF_6$
T [K]	100(1)
M [g/mol]	539.05
crystal system	monoclinic
space group	$P2_1/n$ (No. 14)
a [Å]	10.997(4)
b [Å]	7.771(3)
c [Å]	19.421(8)
β [deg]	91.39(2)
V [Å^3]	1659.2(1)
Z	4
D [g.cm^{-3}]	2.158
crystal size [mm]	0.40 × 0.10 × 0.06
$F(000)$	1060
reflections collected	15701
independent reflections	3352 (R_{int} = 0.051)
observed reflections [$I > 2\sigma(I)$]	3166
completeness to θ = 26.4	98.5%
no. parameters	291
goodness of fit on F^2	1.172
R1, wR2 [$I > 2\sigma(I)$]	0.0382, 0.1061
largest difference peak and hole [e Å^{-3}]	0.86 and −0.88

[a] $R = \sum||F_o| - |F_c||/\sum|F_o|$ for observed reflections, $wR = [\sum w(F_o^2 - F_c^2)^2/\sum wF_o^2]^{1/2}$, $w = 1/(\sigma^2(F_o^2) + 0.025F^2)$, $F = (2F_o + F_c)/3$.

127.2(3)° for Cu1−N1−N2 and 122.1(3)° for Cu2−N2−N1. The Cu1−N1−N2-Cu2 torsion angle is +18.5(3)°. In fact, the connection of Cu^{II} ions, whose octahedra are distorted, should involve a deviation from the *b* axis which is clearly seen on Figure 3a.

The Cu octahedra are oriented in an *ababa* fashion (Figure 2b) as observed for $[Cu(NH_2trz)_3](BF_4)_2 \cdot H_2O$[10] and two other 1D Cu^{II} chain complexes.[7f,11] Other arrangements were found for $[Cu(NH_2trz)_3]SiF_6 \cdot 8/3H_2O$ (*abcabc*)[23] and $[Cu(hyetrz)_3](ClO_4)_2 \cdot 3H_2O$ (*abcbab*).[9]

The Cu···Cu intrachain distance of 3.8850(3) Å is shorter than the Cu···Cu distance found for $[Cu(NH_2trz)_3]A_x \cdot nH_2O$, ($A = BF_4^-$, ($x = 2$, $n = 1$); SiF_6^{2-} ($x = 1$, $n = 8/3$)),[10] with 3.922 Å and 3.904 Å, respectively (Table 3). In $[Cu(hyetrz)_3](CF_3SO_3)_2 \cdot 2H_2O$,[11] there exist three types of Cu^{II} ions, with Cu1···Cu2 = 3.8842(4) Å and Cu2···Cu3 = 3.9354(4) Å, which reflects a difference between the coordination geometry of two pairs of triple *N1*−*N2*-1,2,4-triazole bridges. A similar situation is found for $[Cu(hyetrz)_3](ClO_4)_2 \cdot 3H_2O$ with two types of distances at 3.853(2) Å for Cu1···Cu2 and 3.829(2) Å for Cu2···Cu3. These distances are a little shorter than the ones observed in **11**, which gives a very slight zigzag arrangement to the chain. This can also be seen by the value of the angle between the vectors of Cu^{II} pairs ions, (Cu1, Cu2) and (Cu2, Cu3) which is 175°. For $[Cu(hyptrz)_3]$(4-chloro-3-nitrophenylsulfonate)$_2 \cdot 2H_2O$ (hyptrz = 4-(3′-hydroxypropyl)-1,2,4-triazole),[7f] the Cu1···Cu2 distance increases up to 3.962 Å.

Non-coordinated species are also found in the crystal packing (Figure 3a). A hexafluorozirconate anion is connected to the amino group of the triazole through hydrogen bonding. In addition, the fluorine atoms allow interchain interactions though the connection to nitrogen atoms belonging to two different chains. The involvement of the counteranion in the H-bonding network is probed

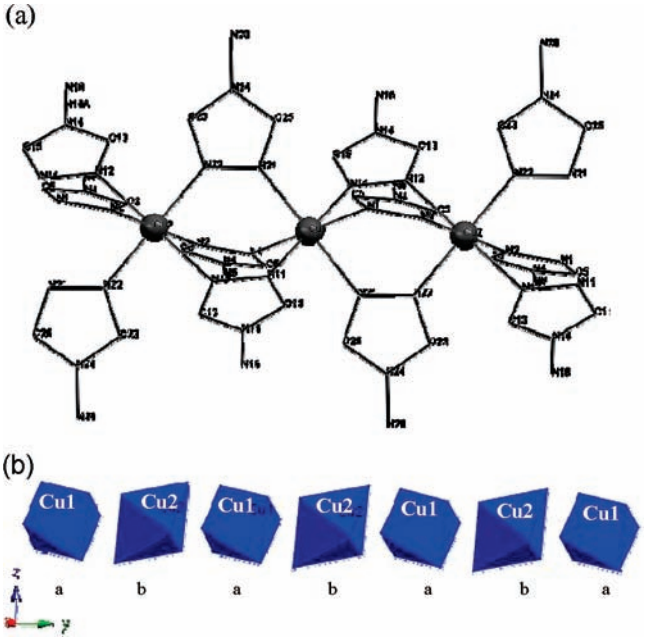

Figure 2. (a) Drawing and atomic labeling system showing the 1D chain of $[Cu(NH_2trz)_3]ZrF_6 \cdot H_2O$ along the *a*-axis. Non-coordinated counteranions and water molecules have been omitted for clarity. (b) Orientation of CuN_6 octahedra in a $[Cu(NH_2trz)_3]ZrF_6 \cdot H_2O$ chain.

by its distortion parameter $\Sigma = 22.05(5)°$ that was determined following ref 25. Indeed, there are two intermolecular interactions between fluoride and the non-coordinated water molecule, (O1−H−F2 and F4), but both fluorine F2 and F4 are linked to N6 and N16, respectively. There is one hydrogen bond between the water molecule and the amino group of the triazole at 2.836 Å, O1···N6 (Table 2b). Water molecules also connect two metallic sites by C−H···O interactions through the triazole rings (Figure 3b). It is found at 2.12 Å (C5−H5···O1) and at 2.20 Å (C3−H3···O1). Thus, these interactions set up a dense hydrogen bonding network.

2.3. Thermal Spin-Crossover Properties. 2.3.1. SQUID Magnetometry. Magnetic susceptibility data for (**1**, **2**, **9**, **10**) were recorded over the temperature range 70−300 K range, and over 4−300 K for **3**−**8**. The magnetic data of all compounds were converted to the HS molar fraction $\gamma_{HS}(T)$ by means of eq (a) and are displayed on Figure 4:

$$\gamma_{HS} = \frac{\chi_M T - \chi_M{}^{LS}(T)}{\chi_M{}^{HS}(T) - \chi_M{}^{LS}(T)} \qquad \text{(a)}$$

$\chi_M{}^{LS}(T) = 184.10^{-6}$ cm^3 mol^{-1},[26] and $\chi_M{}^{HS}$(T) is the paramagnetic susceptibility determined by fitting the susceptibility data in the HS region with the Curie law.

On cooling, compounds **1**−**10** reveal an abrupt hysteretic ST. At room temperature, **1**−**4** are fully HS. γ_{HS} first decreases slightly to ~235 K, and more abruptly down to ~100 K reaching ~0.17 for **1** and 0.22 for **2**, indicating an incomplete ST. The transition temperatures on slow cooling and warming are $T_{1/2}{}^{\downarrow} = 194$ K and $T_{1/2}{}^{\uparrow} = 200$ K for **1**, and $T_{1/2}{}^{\downarrow} = 189$ K and $T_{1/2}{}^{\uparrow} = 196$ K for **2**,

(25) Marchivie, M.; Guionneau, P.; Letard, J. F.; Chasseau, D. *Acta Crystallogr.* **2005**, *B61*, 25.

(26) Carlin, K. D.; van Duynevedt, A. J. *Magnetic properties of transition metal compounds*; Springer-Verlag: New York, 1977.

Table 2. (a) Selected Bond Distances (Å) and (b) Inter-Atomic Distances (up to 3.2 Å) and Angles (deg) for Hydrogen Bonds Interactions in $[Cu(NH_2trz)_3]ZrF_6 \cdot H_2O$ (**11**)

		N11−N12	1.388(4)
Cu1···Cu2	3.8850(3)	N11−C15	1.310(4)
		N12−C13	1.311(4)
bond lengths		N14−C13	1.345(4)
Cu1−N1	2.299(3)	N14−N16	1.417(4)
Cu1−N21	2.080(3)	N14−C15	1.351(4)
Cu2−N2	2.023(3)	N21−N22	1.374(4)
Cu2−N12	2.385(3)	N21−C25	1.317(4)
Cu2−N22	2.029(3)	N22−C23	1.322(4)
Cu1−N11	2.014(3)	N24−N26	1.415(4)
		N24−C25	1.352(4)
		C23−N24	1.346(4)

D−H	D−H	H···A	<DHA	D···A	A
N6−H6A	0.87	2.00	163	2.845	F4
N6−H6B	0.77	2.21	154	2.924	F2 [x, $y-1$, z]
N16−H16A	0.84	2.06	166	2.882	F5 [x, $y-1$, z]
N16−H16B	0.87	2.08	166	2.924	F4 [$-x+3/2$, $y-1/2$, $-z+1/2$]
N26−H26A	0.84	2.10	156	2.888	F3 [$x+1$, y, z]
N26−H26A	0.84	2.58	122	3.109	F1 [$-x+3/2$, $y-1/2$, $-z+1/2$]
N26−H26B	0.95	1.89	171	2.835	F1 [$x+1$, $y-1$, z]
O1−H100	0.90	1.94	169	2.836	N6 [$-x+1$, $-y-1$, $-z$]
O1−H101	0.93	2.00	146	2.824	F2 [x, $y-1$, z]
O1−H101	0.93	2.34	130	3.029	F4 [x, $y-1$, z]
C3−H3	0.95	2.19	152	3.066	O1 [x, $1+y$, z]
C5−H5	0.95	2.12	176	3.067	O1 [x, y, z]

respectively. The ST of **3** and **4** is more complete at the lowest temperature investigated and shifted upward with $T_{1/2}{}^{\downarrow} = 208$ K and $T_{1/2}{}^{\uparrow} = 226$ K for **3**, and $T_{1/2}{}^{\downarrow} = 214$ K and $T_{1/2}{}^{\uparrow} = 238$ K for **4**, respectively. Contrary to all other compounds, only 85% HS Fe^{II} ions are found over a plateau region 300−230 K for **5**, after which γ_{HS} decreases abruptly at $T_{1/2}{}^{\downarrow} = 211$ K and then smoothly down to 18% at 100 K indicating an incomplete ST. On warming the hysteresis is found at $T_{1/2}{}^{\uparrow} = 225$ K. The ST curve of **6** is shifted upward by 12 K, compared to **5** with $T_{1/2}{}^{\downarrow} = 226$ K and $T_{1/2}{}^{\uparrow} = 242$ K. The ST of **7** and **8** occurs around 180 K. **8** displays the most gradual SCO of the series with $T_{1/2}{}^{\downarrow} = 172$ K and $T_{1/2}{}^{\uparrow} = 174$ K, with ∼30% Fe^{II} HS active sites at 100 K. **7** presents a more abrupt ST but still incomplete with $T_{1/2}{}^{\downarrow} = 176$ K and $T_{1/2}{}^{\uparrow} = 184$ K. **9** and **10** presents similar incomplete SCO behavior with a small hysteresis width (**9**: $T_{1/2}{}^{\uparrow} = 211$ K, $T_{1/2}{}^{\downarrow} = 209$ K; **10**: $T_{1/2}{}^{\uparrow} = 205$ K, $T_{1/2}{}^{\downarrow} = 204$ K). The lowering in γ_{HS}, recorded below 25 K for **3**−**8** can be attributed to zero-field splitting but antiferromagnetic interactions between HS Fe^{II} ions cannot be fully excluded.[27] A careful analysis of the low temperature tail of the magnetic curves of compounds **3**−**6** and **8** evidence no freezing-in effect, as recently discovered on $[FeL_3](PF_6)_2$ with L = 2-[3-(2′-pyridyl)pyrazole-1-ylmethyl]pyridine].[28]

2.3.2. ^{57}Fe Mössbauer Spectroscopy. Mössbauer spectra of Fe^{II} compounds (**1**−**10**) were recorded on cooling and warming over the temperature range 78−300 K. Figure 5 shows representative spectra for compound **4**. Mössbauer parameters are listed in Table 4 and in the supplementary section for all other compounds (Supporting Information, Tables S1−S9). The spectrum at 78 K shows two quadrupole doublets attributed to HS Fe^{II} ions ($\delta^{HS} = 1.15(1)$ mm·s^{-1} and $\Delta E_Q{}^{HS} = 3.41(2)$ mm·s^{-1}) and LS Fe^{II} ions ($\delta^{LS} = 0.53(1)$ mm·s^{-1} and $\Delta E_Q{}^{LS} = 0.29(1)$ mm·s^{-1}) in population 7/93, indicating an incomplete ST in good agreement with magnetic susceptibility measurements (Figure 4a). This latter value that represents the lattice contribution to the electric field gradient reveals the presence of local distortions as expected within a constrained chain where some Fe^{II} ions have not been switched.[22] Upon warming, the relative intensity of the HS doublet slowly increases until 183(1) K to reach ∼15%, and then more abruptly. At 300 K, the spectrum consist of only one HS doublet ($\delta^{HS} = 1.05(1)$ mm·s^{-1} and $\Delta E_Q{}^{HS} = 2.77(1)$ mm·s^{-1}). On cooling from room temperature to 78 K, the reverse situation is observed. The spectra shown on cooling and warming modes at 243 and 183 K clearly evidence a hysteresis effect. Indeed, the ST curve deduced by plotting the variation of the temperature dependence of A_{HS}/A_{tot} shows a hysteresis loop, with $T_{1/2}{}^{\downarrow} = 179$ K and $T_{1/2}{}^{\uparrow} = 206$ K (Figure 6). Other compounds also reveal incomplete and hysteretic SCO behavior over the temperature range 300−50 K as shown in Figure 6. These curves were transformed in γ_{HS} by assuming equal Lamb Mössbauer factors for the LS and HS states. Surprisingly, unusually broad hysteresis loops were derived, sometimes temperature shifted as compared to the $\gamma_{HS}(T)$ curves deduced from SQUID measurements (Figure 4). These features prompted us to revise our hypothesis and to accurately determine f factors for both spin states employing the Debye model.[29] The logarithm of the surface of the Mössbauer peaks shows two temperature domains, as expected for the HS and LS states. The slope is proportional to the Debye temperature, θ_D, which is determined in the two spin states for **1**−**6** (Table 5). Taking into account the respective f factor, we could correct the ST curves (Figure 6) and derive the real ST temperatures (Table 5). No major differences are found except for **2**, **3**, and **5**. The Debye temperatures allow determining the rigidity of these chains in the two spin states. The LS lattice is always more rigid than the HS one since the vibrational frequencies increase during the HS to LS transition as a result of the decrease in the Fe−N bond lengths. For comparison, $\theta_D{}^{HS}$ for **2** and **6** is similar as for $[Fe(NH_2trz)_3](ClO_4)_2$ with $\theta_D{}^{HS} = 188(12)$ K.[30] Overall, the variation of the lattice rigidity, $\Delta\theta_D = \theta_D{}^{LS} - \theta_D{}^{HS}$, accompanying the ST of **1**−**6** is of the same order of magnitude (∼21 K).

Figure 7 shows the evolution of the isomer shift at 78 K in the LS state, $\gamma_{LS}{}^{78K}$ vs $T_{1/2}{}^{\uparrow}$ for $[Fe(NH_2trz)_3]^{2+}$ 1D complexes including monovalent and divalent anions, prepared in aqueous methanol or ethanol. In both cases, a linear decrease of $\gamma_{LS}{}^{78K}$ when increasing $T_{1/2}{}^{\uparrow}$ is observed. This behavior corresponds to an increase of the Fe−N bond covalency when anions of smaller volumes are inserted between the chains, resulting in higher transition temperatures (See Figure 8). This increase in covalency may originate from the chains being brought closer together as a consequence of the insertion of small

(27) Timm, C.; Schollwöck, V. *Phys. Rev. B* **2005**, *71*, 224414.
(28) Mishra, V.; Mukherjee, R.; Linares; Codjovi, J.; Varret, F.; Lawson-Daku, M. *Hyperfine Interact.* **2009**, *188*, 71.
(29) Boukheddaden, K.; Varret, F. *Hyperfine Interact.* **1992**, *72*, 349.
(30) Varnek, V. A.; Lavrenova, L. G. *J. Struct. Chem.* **1995**, *36*, 104.

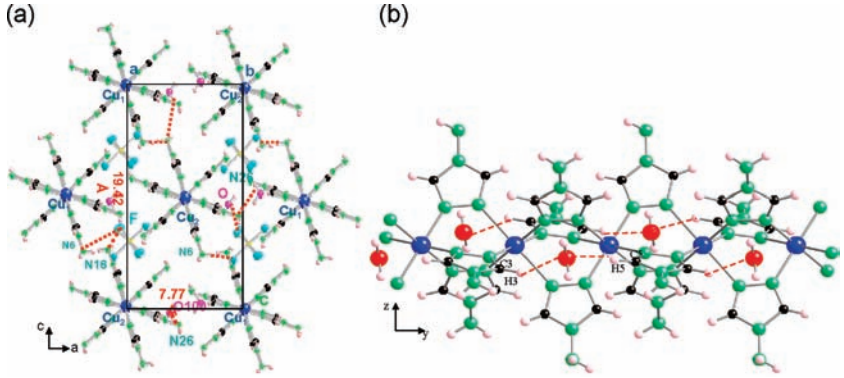

Figure 3. (a) Projection of the crystal structure of $[Cu(NH_2trz)_3]ZrF_6 \cdot H_2O$ on the (*ac*) plane showing hydrogen-bonded chains; (b) view of the cationic chain of $[Cu(NH_2trz)_3]ZrF_6 \cdot H_2O$ along the *b* axis showing intramolecular CH···O interactions involving the water molecules and the triazole ring. On the (*bc*) plane, the H atoms belonging to the amino groups are actually masked by the N atoms.

Table 3. Collection of Crystallographic Data for the $[Cu(NH_2trz)_3]$Anion 1D Chain Complexes

anion	V_{anion} (nm^3)[34]	intrachain Cu ···Cu (Å)	interchain Cu ···Cu (Å)	octahedra arrangement	crystal system	space group	ref.
BF_4^-	0.073	3.922	10.4, 10.6	ab ab ab	triclinic	$P\bar{1}$	(10)
ClO_4^-	0.082	–	–	–	triclinic	$P\bar{1}$	(24)
$BF_4^-/(SiF_6^{-2})_{0.5}$	0.073/0.112	3.877, 3.886	10.3, 11.3, 13.3	ab ab ab	triclinic	$P\bar{1}$	(10)
SiF_6^{-2}	0.112	3.855, 3.886, 3.904	10.5, 11.4, 12.3	abc abc	monoclinic	$P\bar{1}$	(10)
ZrF_6^{-2}	0.121	3.885	10.99, 11.04, 11.70	ab ab ab	triclinic	$P2_1/n$	[a]

[a] This work.

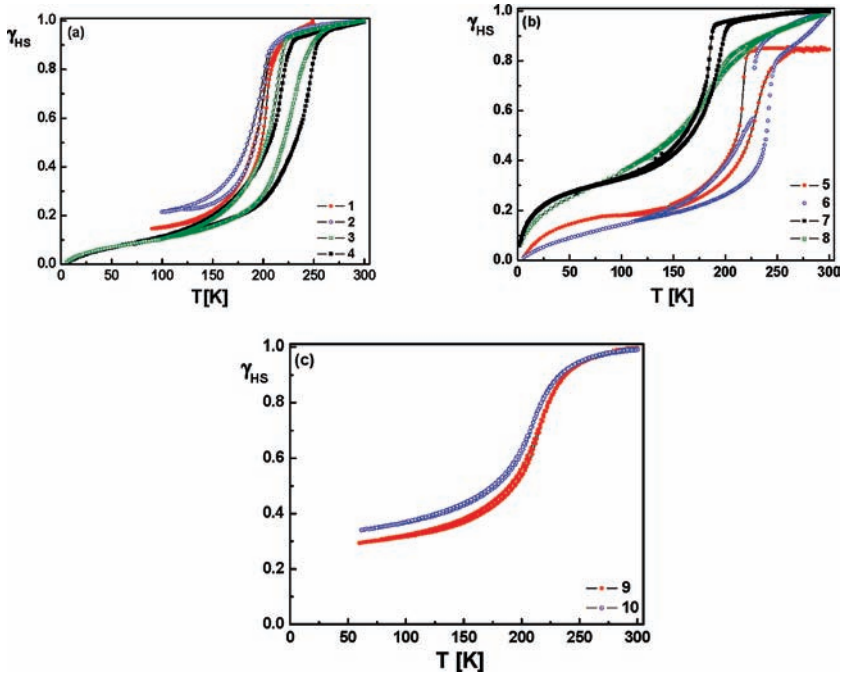

Figure 4. γ_{HS} vs *T* curves on cooling and warming modes for $[Fe(NH_2trz)_3]$Anion$\cdot nH_2O$ complexes (a) **1**−**4**; (b) **5**−**8**; (c) **9**, **10**, as deduced from magnetic susceptibility measurements.

guest anions. As a result, the local distortion of the FeN_6 octahedron increases as seen on Figure 9b for $\Delta E_Q{}^{HS}$ (295 K). It is worth noting that in the LS state, $\Delta E_Q{}^{LS}$ remains constant at 0.30(1) mm/s (Figure 9a). Because there is no valence contribution to consider, the lattice contribution to the quadrupole splitting indicates that the Fe^{II} sites are distorted, as expected for such metal centers connected within a chain by 3 *N*1,*N*2−1,2,4-triazole bridges. A ^{57}Fe Mössbauer spectrum was also recorded on $[Fe_3(NH_2trz)_{10}(H_2O)_2](SbF_6)_6 \cdot 1.5CH_3OH$ (**12**) at 143 K (Figure 10). This spectrum was fitted best by taking into account 3 quadrupole doublets. The central signal corresponds to LS Fe^{II} ions ($\delta^{LS} = 0.53(1)$ mm$\cdot$s^{-1} and $\Delta E_Q{}^{LS} = 0.27(1)$ mm$\cdot$s^{-1}) after switching whereas the two other signals correspond to HS Fe^{II} ions ($\delta^{HS1} = 1.43(1)$ mm$\cdot$s^{-1} and $\Delta E_Q{}^{HS1} = 3.76(2)$ mm$\cdot$s^{-1}, $\delta^{HS2} = 1.19(1)$ mm$\cdot$s^{-1} and $\Delta E_Q{}^{HS2} = 3.57(1)$ mm$\cdot$s^{-1}). The relative area fraction of these signals of 70/15/15 does

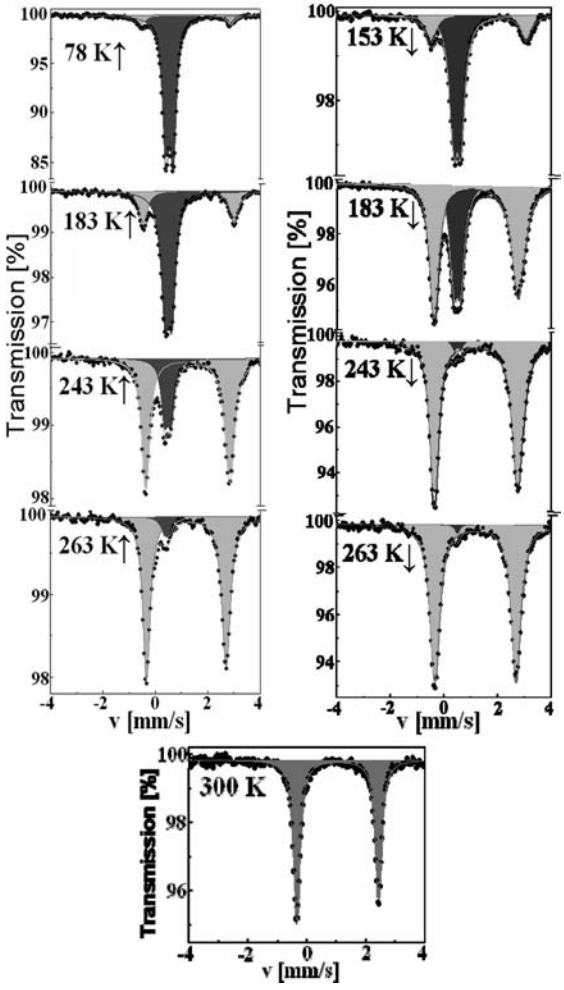

Figure 5. Selected ^{57}Fe Mössbauer spectra of **4** on warming (left) and cooling modes (right). Gray and dark gray correspond to the HS and LS doublets, respectively.

not correspond to the LS/HS1/HS2 spin population because of the Debye−Waller factor differences of the spin states in this system.

An incomplete ST was systematically observed at low temperature for the chain compounds **1**−**10**. This character could originate from crystal defects nearby the ends of chains resulting from an imperfect packing of the polymeric chains, HS inactive FeN_6 sites, or water molecules in the coordination sphere of ends of chains. A closer look at the Mössbauer spectra of **1**−**10** at 78 K reveals only one Fe^{II} site being in the LS and HS states (Figure 5 for **4** and Supporting Information, Figure S1 for **2**, **9**, **8**). Thus, there is no indication of an FeN_3O_3 environment which would be characteristic of three terminal coordinated water molecules[31] provided these are present in sufficient concentration. Nevertheless, ends of polymeric chains with less coordinated water molecules may not be detected by Mössbauer spectroscopy[32] and thus cannot be a priori excluded. However, none of these species are distinguished in our Mössbauer spectra contrary to what is found for the trinuclear complex **12** that clearly reveals two lattice sites: a SCO one and a HS one corresponding to a FeN_5O core with one coordinated water molecule at the extremity of the oligomer (Figure 10).

Table 4. Overview of the ^{57}Fe Mössbauer Parameters for **4** on Warming and Cooling Modes over the Temperature Range 78−300 K

T [K]	δ^a [mm/s]	$\Delta E_Q{}^b$ [mm/s]	$\Gamma/2^c$ [mm/s]	relative area [%]	sites
78(1) ↑	1.15(1)	3.41(2)	0.17(1)	7	HS
	0.53(1)	0.29(1)	0.15(1)	93	LS
100(1) ↑	1.16(1)	3.40(1)	0.18(3)	7.7	HS
	0.52(2)	0.29(1)	0.14(2)	92.3	LS
110(1) ↑	1.14(1)	3.40(1)	0.16(2)	7.0	HS
	0.52(1)	0.29(2)	0.15(1)	93.0	LS
120(1) ↑	1.13(2)	3.42(3)	0.17(2)	7.0	HS
	0.52(1)	0.28(2)	0.15(1)	93.0	LS
160(1) ↑	1.13(3)	3.33(3)	0.18(1)	12.0	HS
	0.51(1)	0.28(3)	0.14(1)	88.0	LS
183(1) ↑	1.11(1)	3.25(1)	0.16(1)	15.3	HS
	0.50(2)	0.27(1)	0.15(3)	84.7	LS
220(1) ↑	1.09(1)	3.08(1)	0.15(1)	43.0	HS
	0.48(1)	0.27(1)	0.13(1)	57.0	LS
240(1) ↑	1.08(1)	3.01(1)	0.14(1)	82.0	HS
	0.47(1)	0.26(1)	0.14(1)	18.0	LS
260(1) ↑	1.07(1)	2.91(1)	0.13(1)	96.0	HS
	0.40(2)	0	0.14(2)	4.0	LS
263(1) ↑	1.18(1)	3.03(1)	0.18(1)	96.3	HS
	0.7[d]	0.2[d]	0.51(5)	3.7	LS
280(1) ↑	1.05(1)	2.83(1)	0.14(5)	100.0	HS
300(1)	1.05(1)	2.77(1)	0.13(1)	100.0	HS
263(1) ↓	1.16(1)	3.03(1)	0.21(1)	98.8	HS
	0.52(6)	0	0.10(1)	1.2	LS
243(1) ↓	1.21(3)	3.11(1)	0.21(1)	98.1	HS
	0.54(7)	0.24(1)	0.10(1)	1.9	LS
223(1) ↓	1.22(1)	3.19(1)	0.22(1)	95.0	HS
	0.57(3)	0.29(2)	0.13(2)	5.0	LS
203(1) ↓	1.24(8)	3.28(2)	0.23(5)	70.3	HS
	0.51(2)	0.25(1)	0.15(9)	29.7	LS
183(1) ↓	1.21(2)	3.14(2)	0.23(1)	65.0	HS
	0.51(3)	0.24(3)	0.2[d]	35.0	LS
163(1) ↓	1.27(2)	3.44(2)	0.24(1)	31.0	HS
	0.52(1)	0.26(1)	0.22[d]	69.0	LS
120(1) ↓	1.12 (2)	3.42(2)	0.20(1)	9.1	HS
	0.55(2)	0.27(1)	0.15(1)	90.9	LS

[a] δ = isomer shift relative to α-iron. [b] ΔE_Q = quadrupole splitting. [c] $\Gamma/2$ = half width at half-maximum. [d] Fixed parameters. ↓ Cooling. ↑ Warming.

2.3.3. Differential Scanning Calorimetry (DSC). Compounds **1**−**10** were investigated by differential scanning over the temperature range 100−295 at 5 K/min for both cooling and heating rates. Representative heat and cooling capacity profiles are depicted in Figure 11. An endothermic peak is observed on warming for **1** at $T_{max}{}^{\uparrow}$ = 210 K and an exothermic peak is recorded at $T_{max}{}^{\downarrow}$ = 200 K, on cooling, thus revealing a hysteresis loop (10 K). These peaks correspond to the first-order phase transition associated to the SCO behavior of **1**. The hysteresis width matches rather well the one recorded by magnetic susceptibility measurements (6 K). It is however, in comparison, temperature shifted because of the different heating and cooling rates used for the calorimetric experiments. All compounds present the same behavior except **6** for which a broad satellite peak is associated to the main exothermic peak. This technique allowed us to confirm the gradual character of the SCO behavior (e.g., **7**, **10**) by the observation of broad peaks. The hysteresis width as well as thermodynamic parameters derived from these

(31) Garcia, Y.; Guionneau, P.; Bravic, G.; Chasseau, D.; Howard, J. A. K.; Kahn, O.; Ksenofontov, V.; Reiman, S.; Gütlich, P. *Eur. J. Inorg. Chem.* **2000**, 1531.
(32) Thomman, M.; Kahn, O.; Guilhem, J.; Varret, F. *Inorg. Chem.* **1994**, *33*, 6029.

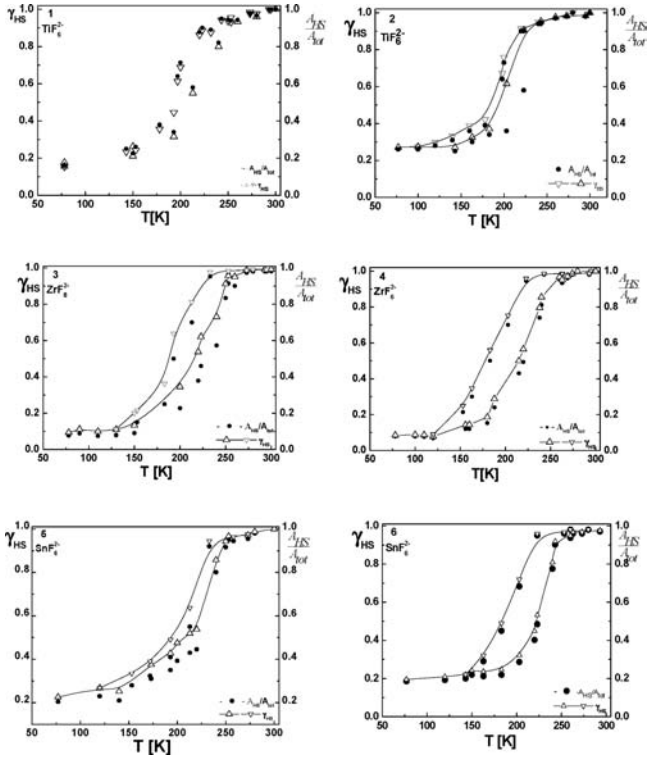

Figure 6. Overview of selected γ_{HS} vs T curves as deduced from Mössbauer spectroscopy, before (●) and after (▲,▼) Debye−Waller corrections for **1**−**6**. The line is a guide to the eyes after corrections.

measurements (ΔH_{HL}, ΔS_{HL}, ΔS_{vib}) are listed in Table 6. Note that the enthalpy values were evaluated taking into account the active Fe^{II} ions only, as deduced by Mössbauer spectroscopy, to strictly refer to SCO sites. The entropy gain is much larger than the characteristic value for the electronic contribution to the entropy (R ln 5 = 13.4 J/mol K) which indicates a contribution to the change in the frequencies of the vibrational modes.[1] Such values are, however, not sufficiently high to suggest another transition type, such as an order−disorder transition of the anion for instance, as earlier noted for $[Fe(NH_2trz)_3]SnF_6 \cdot 0.5H_2O$.[33]

2.4. Diffuse Reflectivity Measurements under Hydrostatic Pressure. The temperature dependence of the normalized reflectivity at the excitation wavelength of 550 nm was investigated over the pressure range (1 bar to 1.7 kbar) for compounds **3** and **4** (Figure 12a). At 1 bar, the hysteresis loops are delineated at ($T_{1/2}^{\uparrow}$ = 225(1) K, $T_{1/2}^{\downarrow}$ = 212(1) K and ($T_{1/2}^{\uparrow}$ = 224(1) K, $T_{1/2}^{\downarrow}$ = 212(1) K) for **3** and **4**, respectively. The transition temperatures recorded by optical reflectivity differ from the ones obtained by magnetic and calorimetric measurements because of the difference of recording mode (only the surface is probed) and the acquisition rate is much slower 0.3 K/min. As the pressure is increased, a shift of the hysteresis loops to higher temperatures is observed while their shape is essentially unchanged. This temperature shift is attributed to the increase of the energy difference between the first vibronic levels corresponding to the HS and LS states under pressure because the volume of the LS Fe^{II} ions is smaller.[1] A decrease of the hysteresis width was also observed under pressure as noted on the phase diagram ($T_{1/2}$ vs P) for compounds **3** and **4** (Figure 12b). Extrapolating the $T_{1/2}$ vs P curves, we estimate that the hysteresis width should disappear at a critical pressure of ~7.8 and ~8.5 kbar for **3** and **4**, respectively, provided there are no other effects to consider, such as for instance a structural phase transition. Thus, although the transition temperatures under 1 bar are similar, the critical pressure is different.

To estimate the magnitude of the internal pressure p, introduced by the anions within the chains, the results obtained from reflectance measurements have been coupled to the calorimetric ones. Thus, the enthalpy variation associated to the ST can be written as

$$\Delta H = H\Delta_0 + p\Delta V_{HL} \qquad \text{(b)}$$

with ΔH_0 = 5.8(1) kJ mol^{-1}, our reference enthalpy corresponding to compounds **7** and **8** that do not display any hysteresis loops and present the lower enthalpies of the series.

The volume change associated to the ST, ΔV_{HL}, can be evaluated as 7.25 $Å^3$ from the ($T_{1/2}$−P) phase diagram displayed in Figure 12, where P refers to the external pressure applied to the system, and from the entropy associated to the ST, ΔS_{HL} (Table 6) using the Clausius−Clapeyron relationship (eq [c]):[34]

$$\Delta V_{HL} = \Delta S_{HL} \frac{dT_{1/2}}{dP} \qquad \text{(c)}$$

Thus, using eq [d], we derive the internal pressure that ranges between ~1 and 5 kbar (Table 6).

$$p = \frac{\Delta H - \Delta H_0}{\Delta V_{HL}} \qquad \text{(d)}$$

3. Discussion

The rational design of highly efficient and specific functional SCO materials is now a main area of investigation. Several 1D chain compounds of formula $[Fe(NH_2trz)_3]Anion \cdot nH_2O$ including monovalent or a few divalent counteranions have been synthesized but no rationalization of their ST properties has been proposed up to now. These compounds display thermally induced ST behavior whose working temperature range actually depends on the nature of the counteranion (geometry, H-bonding ability, etc.) and particularly their size. Indeed, relatively small anions, such as NO_3^- [2a] or Br^-,[2b] allow observation of STs around room temperature, for example, whereas bulkier anions (e.g., BF_4^- [2b]) afford SCO at much lower temperatures. A somehow linear trend between the transition temperature $T_{1/2}$ and the anion radii for $[Fe(NH_2trz)_3](Anion)_2 \cdot nH_2O$ was preliminarily suggested by Lavrenova et al.[2] but later invalidated by the same authors.[2e] In the present work, we have carefully investigated the ST of a series of Fe^{II} 1D NH_2trz coordination polymers including new divalent inorganic anions of different size (TiF_6^{2-}, ZrF_6^{2-}, TaF_7^{2-}, SnF_6^{2-}, GeF_6^{2-}) allowing to evidence two linear size regimes to

(33) Garcia, Y.; Ksenofontov, V.; Mentior, S.; Dîrtu, M. M.; Gieck, C.; Bhatthacharjee, A.; Gütlich, P. *Chem.—Eur. J.* **2008**, *14*, 3745.
(34) Ksenofontov, V.; Spiering, H.; Schreiner, A.; Levchenko, G.; Goodwin, H. A.; Gütlich, P. *J. Phys. Chem. Solids* **1999**, *60*, 393.

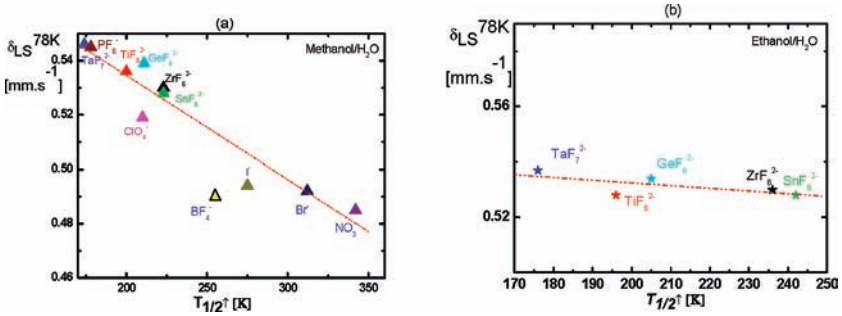

Figure 7. $\delta_{LS}^{(78\ K)}$ vs $T_{1/2}{}^{\uparrow}$ for $[Fe(NH_2trz)_3](Anion)_x$ ($x = 1, 2$) prepared in aqueous (a) CH_3OH or (b) C_2H_5OH. The data for monovalent anions are from ref 14a.

Table 5. Selection of Mössbauer Parameters and Transition Temperatures for $[Fe(NH_2trz)_3]Anion \cdot nH_2O$ (**1**−**10**)

chain	anion	n	synthesis solvent	$\Delta E_Q{}^{HS}$ (295(5) K) [mm s^{-1}]	$\Delta E_Q{}^{LS}$ (78 K) [mm s^{-1}]	γ_{HS} (78 K)	$\theta_D{}^{(HS)}$ [K]	$\theta_D{}^{(LS)}$ [K]	$\Delta\theta_D$ [K]	$T_{1/2}{}^{\uparrow}$ [K]	$T_{1/2}{}^{\downarrow}$ [K]	ΔT [K]
1	TiF_6^{2-}	0.5	MeOH	2.760(1)	0.296(1)	0.16	218(5)	244(5)	26(10)	212	195	17
2	TiF_6^{2-}	1	EtOH	2.763(4)	0.306(2)	0.27	188(5)	209(5)	21(10)	202	192	10
3	ZrF_6^{2-}	0.5	MeOH	2.770(3)	0.293(1)	0.10	122 (5)	148(5)	26(10)	218	190	28
4	ZrF_6^{2-}	0	EtOH	2.794(6)	0.293(1)	0.085	151(5)	171(5)	20(10)	216	179	37
5	SnF_6^{2-}	0.5	MeOH	2.777(2)	0.318(6)	0.23	132(5)	149(5)	17(10)	218	200	18
6	SnF_6^{2-}	1	EtOH	2.784(2)	0.317(2)	0.20	167(5)	184(5)	17(10)	225	189	36
7	TaF_7^{2-}	3	MeOH	2.804(5)	0.292(4)	0.38				199		
8	TaF_7^{2-}	2.5	EtOH	2.785(1)	0.299(2)	0.28				217	217	
9	GeF_6^{2-}	1	MeOH	2.889(5)	0.282(3)	0.32				230		
10	GeF_6^{2-}	0.5	EtOH	2.890(1)	0.280(2)	0.39				223		

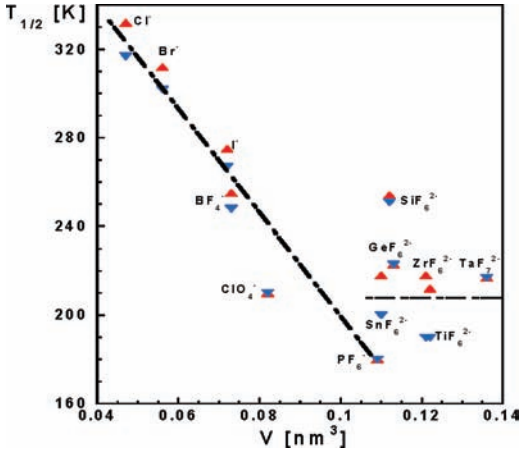

Figure 8. Variation of the transition temperatures, $T_{1/2}$, as deduced from ^{57}Fe Mössbauer spectroscopy, on cooling (▼) and warming modes (▲) vs the anion volume for $[Fe(NH_2trz)_3]\cdot Anion$.

be considered to account for the ST range observation (Figure 8). Here, we consider the variation of $T_{1/2}$ (on cooling and warming) versus the volume of the inserted anion[35] instead of considering the radius only determined from the Kapustinskii's equation.[36] This choice allowed us to take into account the dimensional size of the anions. Two linear regimes are effective: (i) between $0.04 \leq V\ (nm^3) \leq 0.09$, where a decrease of the $T_{1/2}$ is observed with increasing volume. In this volume range, less energy is needed to switch the spin state of the metallic ions as much as we increase in volume and space out the chains. (ii) Above $V \geq 0.11$ nm^3, with a saturation of $T_{1/2} \sim 200$ K. This behavior corresponds to a chain spacing limit in such a way that when the LS−HS transition occurs, FeN_6 sites have enough freedom to increase their bond length and expand along the chain axis, the counteranion being affected very little by the ST itself because of the large distance between a pair of chains where these anions are located. Thus, insertion of a bigger counteranion between the chains decreases the relative vertical displacement of the potential wells, in favor of the HS state, thereby inducing a negative pressure effect. What would be the SCO situation when the anion volume increases further? We extrapolate that the chains would become isolated to each other and that the $T_{1/2}$ would either stay in the same temperature range (~200 K) or decrease thus favoring a fully HS state. This second hypothesis has actually been recently confirmed for the HS 1D chain $[Fe(NH_2trz)_3]B_{10}H_{10}\cdot H_2O$[37] that includes a counteranion of $V \sim 0.23$ nm^3,[38] that is much higher than the one of TaF_7^{2-}, which is the biggest anion investigated in the present study. This compound stays paramagnetic on cooling over the temperature range 300−2 K.

As deduced by comparison of the X-ray powder diffraction patterns recorded at 293 K for compounds **1**−**10** (Figure 1), the insertion of this series of divalent anions does not affect much the structural organization of the chains, allowing to validate complementary spectroscopic comparisons. Indeed, Mössbauer spectroscopy confirms that whatever the inserted divalent anion, the local symmetry of the Fe octahedra is not modified as deduced by the constant value of the quadrupole splitting in the HS state. For lower size anion, a decrease of $\Delta E_Q{}^{HS}$(295 K) is however noted (Figure 9b) thus indicating an increase of the local distortion around the

(35) Donald, H.; Jenkins, B.; Roobottom, H. K. *Inorg. Chem.* **1999**, *38*, 3609.
(36) Yatsimirskii, K. B. *Thermochemistry of Complex Compounds*; Moscow, 1951.
(37) Bushuev, M. N.; Lavrenova, L. G.; Shvedenkov, Y. G.; Varnek, V. A.; Sheludyakova, L. A.; Volkov, V. V.; Larionov, S. V. *Koord. Khim.* **2008**, *34*, 195.
(38) Kaczmarczyk, A.; Dobrott, R. D.; Lipscomb, W. *Chemistry* **1962**, *48*, 729.

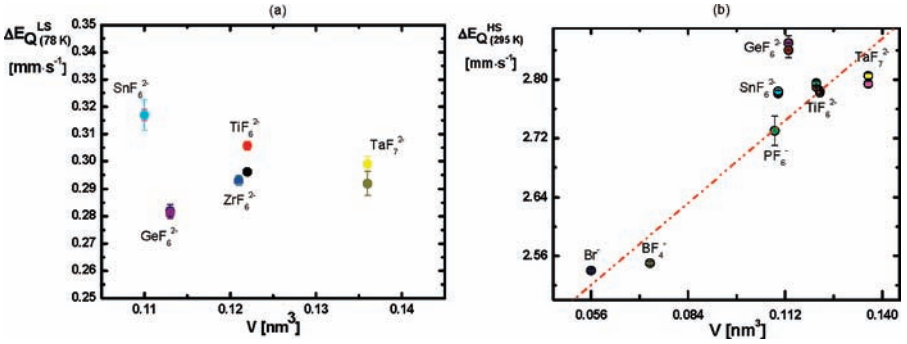

Figure 9. $\Delta E_Q{}^{LS}{}_{(78\ K)}$ vs V [nm^3] (a) and $\Delta E_Q{}^{HS}{}_{(295\ K)}$ vs V [nm^3] (b) for $[Fe(NH_2trz)_3](Anion)_x$ (x = 1, 2) prepared in aqueous CH_3OH. Data from monovalent anions[14a] have been added.

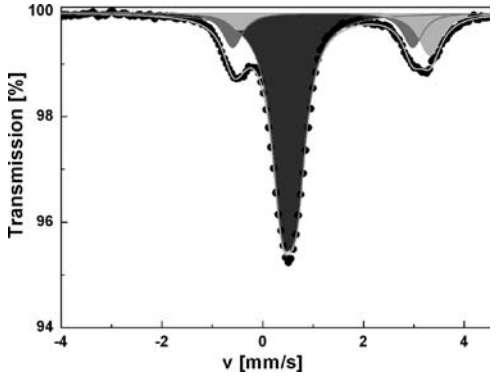

Figure 10. ^{57}Fe Mössbauer spectra at 143 K for $[Fe_3(NH_2trz)_{10}(H_2O)_2](SbF_6)_6\cdot 1.5CH_3OH$ (**13**). Gray and light gray correspond to two HS sites. Dark gray correspond to a LS doublet.

metallic ion. Indeed, it is worth noting that the electric field gradient contribution of the lattice is usually of opposite sign as compared to that of the valence electrons.[39] This increase of local distortion indicates that chains are much closer in the case of lower size anions than for larger size anions. This geometric feature is also seen on the evolution of the isomer shift for the LS state, δ^{LS}, versus $T_{1/2}$ (Figure 7). Indeed, when $T_{1/2}$ increases, that is, when the anion volume decreases (See Figure 8), $\delta_{LS}{}^{78K}$ decreases. Because the isomer shift is of opposite sign to the electronic density seen by the iron atoms, the covalency degree of the Fe−N bond increases, which is consistent with the chains that are moved closer. Such structural features are deduced by X-ray diffraction when comparing the crystal structures of $[Cu(NH_2trz)_3]A_{2\ or\ 1}\cdot nH_2O$ ($A = BF_4^-$, SiF_6^{2-}) that crystallizes in the $P\bar{1}$ space group.[10] Indeed, when the anion volume increases ($V(BF_4^-) = 0.073$ nm^3 < $V(SiF_6^{2-}) = 0.112$ nm^3 Å), the chain spacing increases (Table 3).

In the absence of suitable single crystals for these Fe^{II} compounds, and to better understand the impact of the supramolecular organization of these materials, the crystal structure of a model compound including a divalent anion of the present series was solved: $[Cu(NH_2trz)_3]ZrF_6\cdot H_2O$ (**11**). The structure is stabilized by a dense hydrogen bonding network, involving the counteranion, ZrF_6^{2-}, located in the third coordination sphere, the amino group of the 1,2,4-triazole ligand, and a non-coordinated water molecule (Figure 3a). More precisely, the anion is linked to both amino group and water molecules and to two 1D chains through the anion setting up interchain interactions. Intrachain interaction is also found because a non-coordinated water molecule establishes a bridge between metallic sites within a chain (Figure 3b), as noted for $[Cu(tba)_3](CF_3SO_3)_2\cdot 3H_2O$ (tba = *N*-(4*H*-1,2,4-triazole-4-yl)benzamide.[40,41] Such supramolecular interactions may well play an effective role in the propagation of elastic cooperative interactions within **3** resulting in the observation of a wide hysteresis loop of 28 K (Figure 4a). Such an extended 3D hydrogen bonding network was also suggested to account for the 35 K hysteresis width of $[Fe(NH_2trz)_3](NO_3)_2$.[15] These results thus point out the high potential of H-bonds for transmitting cooperative interactions during a ST as recently highlighted for a structurally characterized Fe^{II} mononuclear SCO compound that displays a 70 K wide thermal hysteresis loop.[42] We thus cannot separate the influence of H-bonding[2e] from the size effect of the anions on the SCO behavior of the Fe derivatives because the selected fluoride anions could favor extended H-bonding networks as found in the crystal structure of **11**.

We can also comment on the nature of the inserted anions in this system. It is of interest to note that ^{119}Sn, ^{73}Ge, and ^{121}Sb atoms are Mössbauer active and could thus give relevant information on the crystal lattice in the LS and HS states of these SCO compounds, thus acting as nuclear sensors. Already, we have recently gained insight to the internal pressure felt by the counteranion during the SCO of chain compounds by accurately following the temperature dependence of its local distortion in $[Fe(NH_2trz)_3]SnF_6\cdot 0.5H_2O$ by ^{119}Sn Mossbauer spectroscopy. We could observe that the octahedron is distorted below $T_{1/2}$ and becomes regular above it, thereby demonstrating that the anion is able to feel the spin state crossover despite its localization external to the chains.[33] It is finally of interest to note that it is the first time that Zr, Ge, Ti, and Ta based anions are inserted in SCO compounds, thus affording a new generation of inorganic precursors that could be used in the future syntheses of SCO systems and extending the panel of anions usually employed in SCO research such as BF_4^-, ClO_4^- and PF_6^-, to name a few.

Hydrostatic pressure measurements were carried out on selected SCO compounds, **3** and **4**. Under pressure the chains are expected to get closer to each other, which should increase the connections in the crystal lattice and render the transition

(39) Ingalls, R. *Phys. Rev.* **1964**, *133*, A787.

(40) Seredyuk, M.; Gaspar, A. B.; Muñoz, M. C.; Verdaguer, M.; Villain, F.; Gütlich, P. *Eur. J. Inorg. Chem.* **2007**, *28*, 4481.

(41) Seredyuk, M.; Gaspar, A. B.; Ksenofontov, V.; Galyametdinov, Y.; Verdaguer, M.; Villain, F.; Gütlich, P. *Inorg. Chem.* **2008**, *47*, 10232.

(42) Weber, B.; Bauer, W.; Obel, J. *Angew. Chem., Int. Ed.* **2008**, *47*, 10098.

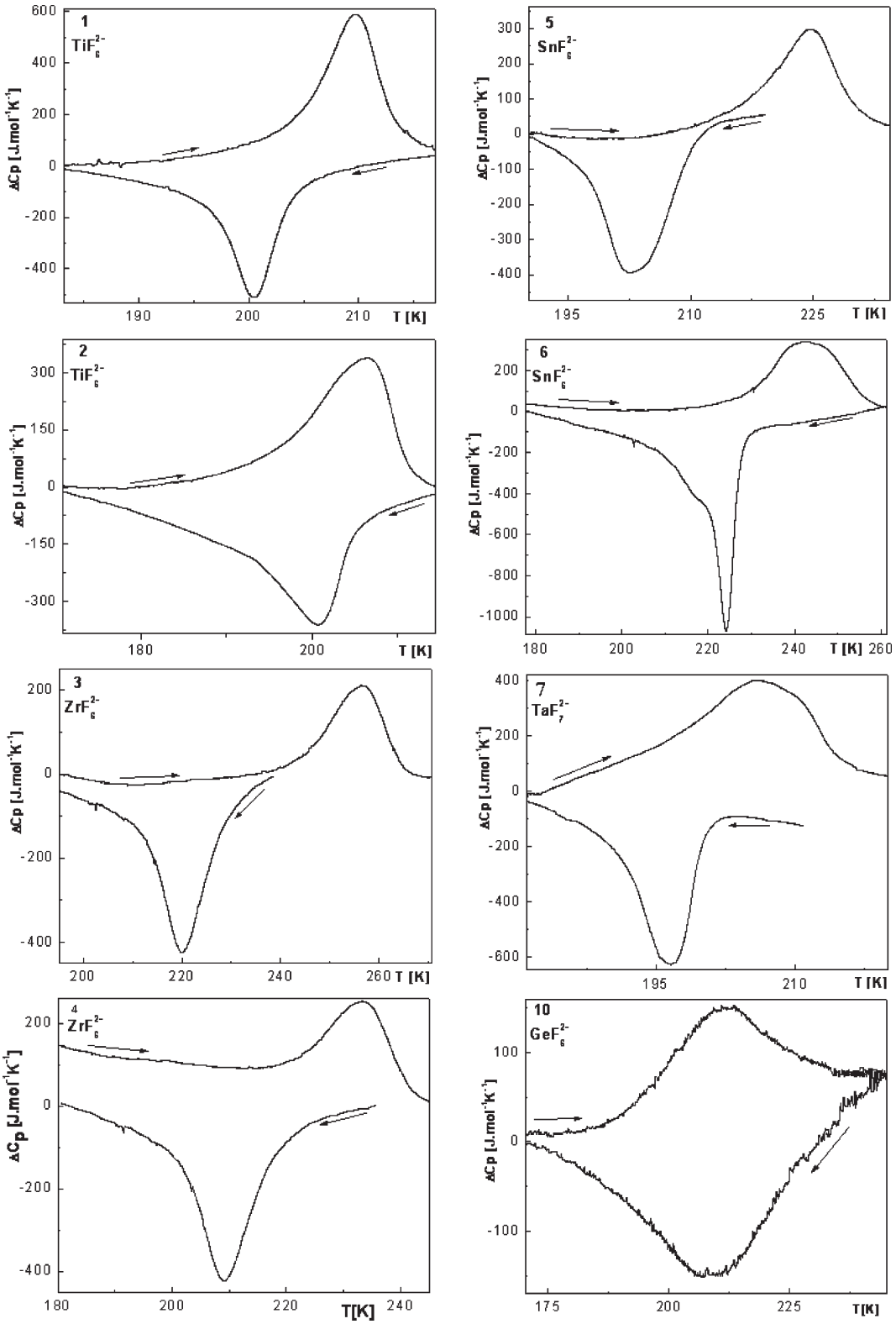

Figure 11. Selected DSC profiles for $[Fe(NH_2trz)_3]$Anion (**1**−**7**, **10**) in the 100−295 K temperature range in the cooling and warming modes.

more abrupt. The steepness of the transition curves is, however, preserved whatever the applied pressure which indicates that the chain character is maintained.[43] The slopes of the $T_{1/2}$ versus P line, $dT_{1/2}/dP = 11.7(5)$ K kbar^{-1} and 13.6 (5) K kbar^{-1} for **3** and **4**, respectively, are similar to the one observed for the mononuclear compound $[Fe(2\text{-pic})_3]Cl_2 \cdot$ EtOH (2-pic = 2-picolylamine)[44] but lower than the one

(43) Garcia, Y.; Van Koningsbruggen, P. J.; Lapouyade, R.; Fournès, L.; Rabardel, L.; Kahn, O.; Ksenofontov, V.; Levchenko, G.; Gütlich, P. *Chem. Mater*. **1998**, *10*, 2426.

(44) Köppen, H.; Müller, E. W.; Köhler, C. P.; Spiering, H.; Meissner, E.; Gütlich, P. *Chem. Phys. Lett*. **1982**, *91*, 348.

Table 6. Transition Temperatures As Deduced from DSC Measurements, Thermodynamic Parameters, Chain Lengths, and Transition Temperatures for **1-10**

entry	$T_{max}^{\uparrow}$ (K)	$T_{max}^{\downarrow}$ (K)	ΔT (K)	as (%)[a]	ΔH_{HL} (kJ mol^{-1})	ΔS_{HL} (J mol^{-1} K^{-1})	ΔS_{vib} (J mol^{-1} K^{-1})	N^b	τ (nm)[c]	p (kbar)[d]
1	210	200	10	72	7.1	34.5	21.1	7	2.15	2.7
2	206	201	5	75	7.3	36	22.6	8	2.50	3.4
3	233	209	24	85	7.4	33.6	20.2	13	4.30	3.6
4	256	220	36	85	6.7	30.5	17.1	13	4.30	1.8
5	224	203	21	75	6.3	31.2	17.8	8	2.50	0.9
6	244	224	20	80	8	34.3	20.9	10	3.58	5.0
7	206	197	9	72	5.9	30	17	7	2.15	p_0
8		200		60	5.8	29	16	5	1.43	p_0
9	213	211	2	62	6.4	30	17	5	1.43	1.1
10	213	207	6	58	6.9	32	19	5	1.43	2.5

[a] as = active sites. [b] Number of atoms in a chain. [c] τ = chain length. [d] = electrostatic pressure.

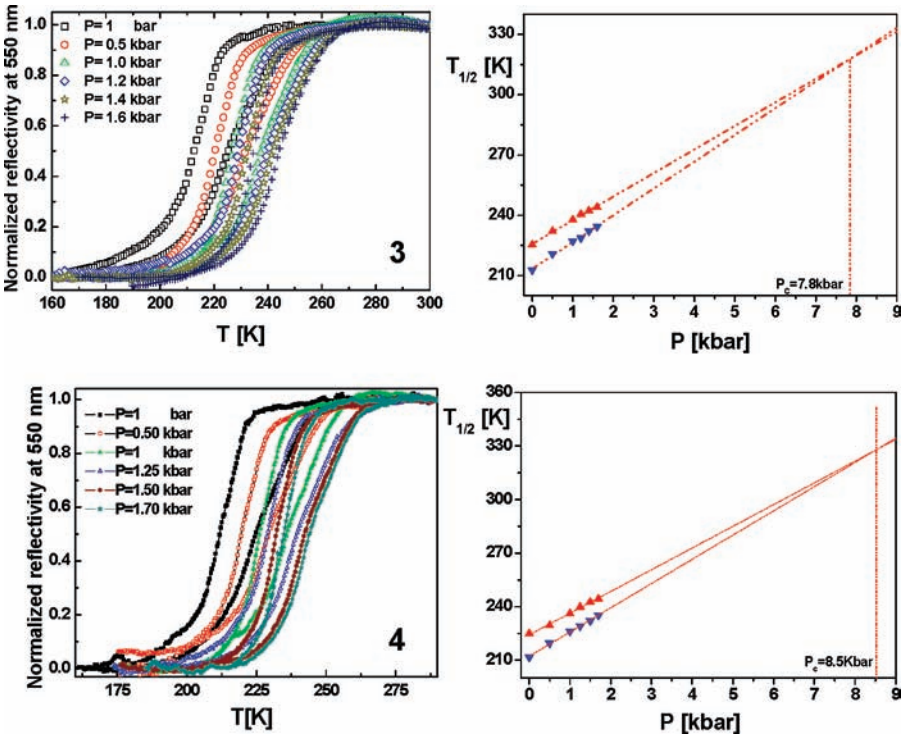

Figure 12. (a) Normalized reflectivity at 550 nm vs T over the temperature range 100−300 K on cooling and warming at several pressures (1 bar up to 1.7 kbar). (b) Variation of transitions temperatures on warming (▲) and cooling (▼) vs P for $[Fe(NH_2trz)_3]ZrF_6 \cdot 0.5H_2O$ (**3**) (top) and $[Fe(NH_2trz)_3]ZrF_6$ (**4**) (bottom). The dotted line indicates the pressure at which the hysteresis loop disappears.

found for the 1D chain [Fe(hyetrz)$_3$](3-nitro-phenylsulfonate)$_2$ (24 K kbar^{-1})[43] and the 2D ST compound [Fe(btr)$_2$(NCS)$_2$]·H$_2$O (btr = 4,4′-bis-1,2,4-triazole)[45] (19.0(5) K kbar^{-1}) that was also studied by diffuse reflectivity.[46] Interestingly, a decrease of the hysteresis width is observed, which may indicate a weakening of supramolecular interactions for this system, in particular intra-chain interactions that were identified for $[Cu(NH_2trz)_3]ZrF_6 \cdot H_2O$ (Figure 3b). Hysteresis decrease has been predicted by mean field theory[34] but only once observed for a 1D chain compound, [Fe(hyptrz)$_3$](4-chlorophenylsulfonate)$_2$·H$_2$O (hyptrz = 4-(3′-hydroxy-propyl)-1,2,4-triazole), with an additional reentrance phenomenon.[47]

It is here important to distinguish between the external pressure P that corresponds to a given energy provided to the system (as one can consider the temperature ($T_{1/2}$) necessary to be provided to switch the system from the LS to the HS state) from the electrostatic pressure set up by anion−cation interactions, p, that we have here estimated numerically, for the first time. This pressure can also be regarded, by comparison, as a "chemical pressure"[48−50] because it corresponds to a variation of the composition of the material depending on the nature of the inserted non-coordinated species. This internal pressure is, however, different from the local elastic pressure set up during thermal relaxation after LIESST

(45) Garcia, Y.; Ksenofontov, V.; Levchenko, G.; Schmitt, G.; Gütlich, P. J *Phys. Chem. B* **2000**, *104*, 5045.
(46) (a) Jeftíc, J.; Menendez, N.; Wack, A.; Codjovi, E.; Linares, J.; Goujon, A.; Hamel, G.; Klotz, S.; Syfosse, G.; Varret, F. *Meas. Sci. Technol.* **1999**, *10*, 1059. (b) Tanasa, R.; Stancu, A.; Letard, J. F.; Codjovi, E.; Linares, J.; Varret, F. *Chem. Phys. Lett.* **2007**, *443*, 435.
(47) Garcia, Y.; Ksenofontov, V.; Levchenko, G.; Gütlich, P. *J. Mater. Chem.* **2000**, *10*, 2274.
(48) Schenker, S.; Hauser, A.; Wang, W.; Chan, I. Y. *Chem. Phys. Lett.* **1998**, *297*, 281.
(49) Hauser, A.; Amstutz, N.; Delahaye, S.; Sadeli, A.; Schenker, S.; Sieber, R.; Zerara, M. *Chimia* **2002**, *56*, 685.
(50) Jeftíc, J.; Ecolivet, C.; Hauser, A. *High Pressure Res.* **2003**, *23*, 359.

irradiation and that is induced by the neighboring spin changing molecules as described by Hauser.[51]

It is of interest to note that a large internal pressure range is found for the investigated compounds (Table 6). This is not surprising because a tiny change in the nature or number of non-coordinated species can dramatically modify the transition temperature.[20,43] The number of atoms in a chain, N, also reported in Table 6, has been evaluated following eq e:[52]

$$N = 2\left(\frac{100}{100-\mathrm{as}}\right) \qquad \text{(e)}$$

where as is the number of active sites undergoing the SCO behavior that has been accurately determined by ^{57}Fe Mössbauer spectroscopy in the higher and lower thermal branches of the ST curves for **1**−**10**. The chains (**3**, **4**) comprising the larger number of atoms {13} display the wider hysteresis loop as expected for longer chains with enhanced cooperative effects. Unfortunately, it was not possible to compare these results with dynamic light scattering data because of the low solubility of the present coordination polymers. Because, the Fe···Fe distance of the cationic chain $[Fe(NH_2trz)_3]^{2+}$ was determined by EXAFS spectroscopy (3.58 Å),[8a] it was possible to estimate for the first time, the chain length distribution τ that ranges between 1 and 4 nm (Table 6).

4. Concluding Remarks

We have shown that the nature and geometry of the counteranions, as well as the chain length, govern the ST behavior of 1D coordination polymers. Because the ST of these materials is accompanied by a dramatic color change, such characteristics could be useful for selecting appropriate candidates for a given application (displays, sensors, etc.) in a certain temperature or pressure working range. The first SCO materials with new fluorinated inorganic anions were presented and included in a database according to their volume. The internal electrostatic pressure of these anions located in the neighboring cationic chains, as well as chain lengths of these coordination polymers, was also estimated.

5. Experimental Section

Syntheses. All reagents and solvents were used as received from commercial sources: hexafluorotitanic acid, 99.9%, 60 wt % solution in water (Aldrich), hexafluorozirconic acid, 45 wt %, solution in water (Aldrich), ammonium hexafluorostanate(IV), 99.99% (Aldrich), ammonium heptafluorotantalate (V), 99.99% (Aldrich) ammonium hexafluorogermanate(IV), 99.99%, (ACROS), iron(II) chloride tetrahydrate 99% (ACROS), iron powder 99.99% (Janssen Chemica), Cu powder, 99.5% (Merck), 4-amino-1,2,4-triazole, 99% (ACROS).

$[Fe(NH_2trz)_3]TiF_6\cdot 0.5H_2O$ (1). Iron powder (0.0857 g, 1.534 mmol) was mixed with 0.1 mL of H_2TiF_6 (1.534 mmol) and stirred at room temperature and in air for 30 min, the solution of which was filtered leading to a green solution of $[Fe(H_2O)_6]TiF_6$. This aqueous precursor solution was added to a hot methanolic solution (5 mL) containing NH_2trz (0.3871 g, 4.6 mmol). A white precipitate was formed immediately and stirred for ∼1 h at room temperature. It was filtered, washed with 5−10 mL of methanol and dried in a desiccator. Yield: 0.61 g, 83%. Anal. for $FeC_6H_{13}N_{12}O_{0.5}TiF_6$ (479 g/mol): calcd C, 15.05; H, 2.74; N, 35.09; Fe, 11.66. Found: C, 15.51; H, 2.80; N, 35.54; Fe, 10.14%. IR (cm^{-1}): $\nu(NH_2)\sim 3305$ (s), $\nu(N-N)\sim 1217$ (s), ν(C−H out of plane) ∼ 1027 (m), ν(C−H ring torsion) = 621 (vs), ν(Ti−F) ∼ 569 (m).

$[Fe(NH_2trz)_3]TiF_6\cdot H_2O$ (2). It was synthesized following the same procedure as for **1** except that warm ethanol was used to dissolve NH_2trz. A white precipitated was obtained. Yield: 0.43 g, 86.5%. Anal. for $FeC_6H_{14}N_{12}OTiF_6$ (488.01 g/mol): calcd C, 14.77; H, 2.89; N, 34.44; Fe, 11.44. Found: C, 15.26; H, 2.59; N, 34.87; Fe, 12,57%. IR (cm^{-1}): $\nu(NH_2)\sim 3318$ (s), ν(N−N) ∼ 1218 (s), ν(C−H out of plane) ∼ 1031 (m), ν(C−H ring torsion) = 624 (vs), ν(Ti−F)∼567 (m).

$[Fe(NH_2trz)_3]ZrF_6\cdot 0.5H_2O$ (3). Iron powder (0.0857 g, 1.534 mmol) was mixed with 0.1 mL of H_2ZrF_6 (1.5 mmol) and stirred at room temperature and in air for 30 min, the solution of which was filtered leading to a pale green solution of $[Fe(H_2O)_6]ZrF_6$. The same procedure was used as for **1** working with NH_2trz dissolved in MeOH, affording a white precipitate. Yield: 0.94 g, 66.4%. Anal. for $FeC_6H_{13}N_{12}O_{0.5}ZrF_6$ (520.97 g/mol): calcd C, 13.80; H, 2.51; N, 32.18; Fe, 10.69. Found: C, 14.36; H, 2.47; N, 32.81; Fe, 9.96%. IR (cm^{-1}): $\nu(NH_2)\sim 3308$ (s), $\nu(N-N)\sim 1218$ (s), ν(C−H out of plane) ∼ 997 (m), ν(C−H ring torsion) = 625 (vs), ν_1(Zr−F)∼590 (m).

$[Fe(NH_2trz)_3]ZrF_6$ (4). It was synthesized following the same procedure as for **3** except that warm ethanol was used to dissolve NH_2trz. A white precipitated was obtained. Yield: 0.64 g, 50%. Anal. for $FeC_6H_{12}N_{12}ZrF_6$ (511.96 g/mol): calcd C, 14.04; H, 2.36; N, 32.75; Fe, 10.88. Found: C, 14.80; H, 2.49; N, 33.03; Fe, 9.65%. IR (cm^{-1}): $\nu(NH_2)\sim 3226$ (m), $\nu(N-N)\sim 1218$ (s), ν(C−H out of plane) ∼ 997 (m), ν(C−H ring torsion) = 624 (vs), ν_1(Zr−F)∼590 (m).

$[Fe(NH_2trz)_3]SnF_6\cdot 0.5H_2O$ (5). $(NH_4)_2SnF_6$ (0.3388 g, 1.26 mmol) dissolved in 10 mL of water was added to a 5 mL of aqueous solution of $FeCl_2\cdot 4H_2O$ (0.2506 g, 1.26 mmol). A pale green solution of $[Fe(H_2O)_6]SnF_6$ was obtained. The same procedure was used as for **1** working with NH_2trz dissolved in MeOH, affording a white precipitate. Yield: 0.38 g, 76%. Anal. for $FeC_6H_{13}N_{12}O_{0,5}SnF_6$ (550.96 g/mol): calcd C, 13.11; H, 2.38; N, 30.57; Fe, 10.16. Found: C, 13.31; H, 2.31; N, 29.84; Fe, 9.80%. IR (cm^{-1}): $\nu(NH_2)\sim$ 3215 (s), $\nu(N-N)\sim$ 1217 (s), ν(C−H out of plane)∼1000 (m), ν(C−H ring torsion) = 612 (s), ν(Sn−F)∼ 601 (m).

$[Fe(NH_2trz)_3]SnF_6\cdot H_2O$ (6). It was synthesized following the same procedure as for **5** except that a warm ethanol was used to dissolve NH_2trz. A white precipitated was obtained. Yield: 0.4 g, 80%. Anal. for $FeC_6H_{14}N_{12}OSnF_6$ (559.96 g/mol): calcd C, 12.90; H, 2.53; N, 30.08; Fe, 9.99. Found: C, 13.04; H, 2.27; N, 29.80; Fe, 9.17%. IR (cm^{-1}): $\nu(NH_2)\sim 3225$ (s), $\nu(N-N)\sim 1217$ (s), ν(C−H out of plane) ∼ 998 (m), ν(C−H ring torsion) = 610 (s), ν(Sn−F)∼ 600 (m).

$[Fe(NH_2trz)_3]TaF_7\cdot 3H_2O$ (7). An aqueous solution (10 mL) containing 0.3176 g of $FeCl_2\cdot 4H_2O$ (1.59 mmol) was added to an aqueous solution (5 mL) containing 0.5591 g of $(NH_4)_2TaF_7$ (1.59 mmol) and ∼ 0.01 g of ascorbic acid. A pale green solution of $[Fe(H_2O)_6]TaF_7$ was obtained. The same procedure was used as for **2** working with NH_2trz dissolved in methanol, affording a white precipitate. Yield: 0.8 g, 74%. Anal. for $FeC_6H_{18}N_{12}O_3TaF_7$ (676.03 g/mol): calcd C, 10.66; H, 2.68; N, 24.86; Fe, 8.26. Found: C, 10.66; H, 1.79; N, 24.44; Fe, 8.84%. IR (cm^{-1}): $\nu(NH_2)\sim 3220$ (s), $\nu(N-N)\sim 1220$ (s), ν(C−H out of plane) ∼ 1000 (m), ν(C−H ring torsion) = 613 (s), ν(Ta−F) ∼ 1394, 536 (m).

(51) (a) Hauser, A. *Chem. Phys. Lett.* **1992**, *192*, 65. (b) Jeftíc, J.; Hauser, A. *Chem. Phys. Lett.* **1996**, *248*, 458. (c) Jeftíc, J.; Hauser, A. *J. Phys. Chem. B* **1997**, *101*, 10262. (d) Hauser, A.; Jeftíc, J.; Romstedt, H.; Hinek, R.; Spiering, H. *Coord. Chem. Rev.* **1999**, *190*−*192*, 471.

(52) (a) Roubeau, O.; Gomez, M. A.; Balskus, E.; Kolnaar, J. J. A.; Haasnoot, J. G.; Reedijk, J. *New J. Chem.* **2001**, *25*, 144. (b) Quesada, M.; Prins, F.; Bill, E.; Kooijman, H.; Gamez, P.; Roubeau, O.; Spek, A. L.; Haasnoot, J. G.; Reedijk, J. *Chem.—Eur. J.* **2008**, *14*, 8486.

$[Fe(NH_2trz)_3]TaF_7 \cdot 2.5H_2O$ (8). It was synthesized following the same procedure as for **7** except that warm ethanol was used to dissolve NH_2trz. A white precipitated was obtained. . Yield: 0.8 g, 81%. Anal. for $FeC_6H_{16.5}N_{12}O_{2.5}TaF_7$ (667.03 g/mol): calcd C, 10.75; H, 2.56; N, 25.08; Fe, 8.37. Found: C, 10.80; H, 2.57; N, 2520; Fe, 9.50%. IR (cm^{-1}): $\nu(NH_2)$ ~3223 (s), ν(N−N) ~1221 (s), ν(C−H out of plane) ~ 1000 (m), ν(C−H ring torsion) = 612 (s), ν(Ta−F)~ 1396, 534 (m).

$[Fe(NH_2trz)_3]GeF_6 \cdot H_2O$ (9). $FeCl_2 \cdot 4H_2O$ (0.2232 g, 1.12 mmol) dissolved in 3 mL of distilled water was added to an aqueous solution (5 mL) of $(NH_4)_2GeF_6$ (0.25 g, 1.12 mmol) with a pinch of ascorbic acid. A pale green solution of $[Fe(H_2O)_6]GeF_6$ was obtained after stirring for a few minutes. The same procedure was used as for **1** working with NH_2trz dissolved in MeOH, affording a white precipitate. 0.5 g, 70%. Anal. for $FeC_6H_{14}N_{12}OGeF_6$ (513.98 g/mol): calcd C, 14.06; H, 2.75; N, 32.78; Fe, 10.89. Found: C, 14.01; H, 2.52; N, 32.19; Fe, 9.92%. IR (cm^{-1}): $\nu(NH_2)$ ~ 3230 (s), ν(N−N) ~ 1217 (s), ν(C−H out of plane) ~ 997 (m), ν(C−H ring torsion) = 624 (s), ν(Ge−F) ~ 600 (s).

$[Fe(NH_2trz)_3]GeF_6 \cdot 0.5H_2O$ (10). It was synthesized following the same procedure as for **9** except that warm ethanol was used to dissolve NH_2trz. A white precipitated was obtained. Yield: 0.45 g, 80%. Anal. for $FeC_6H_{13}N_{12}O_{0.5}GeF_6$ (504.96 g/mol): calcd C, 14.31; H, 2.60; N, 33.37; Fe, 11.09. Found: C, 14.31; H, 2.57; N, 32.38; Fe, 9.94%. IR (cm^{-1}): $\nu(NH_2)$ ~ 3300 (s), ν(N−N) ~ 1217 (s), ν(C−H out of plane) ~ 997 (m), ν(C−H ring torsion) = 621 (s), ν(Ge−F) ~ 603 (s).

$[Cu(NH_2trz)_3]ZrF_6 \cdot H_2O$ (11). A 5 mL portion of aqueous solution of $[Cu(H_2O)_6]ZrF_6$ was obtained by stirring copper powder 0.0455 g (0.7 mmol) with 0.22 mL (0.72 mmol) of H_2ZrF_6 at room temperature for 30 min, the solution of which was filtered leading to a pale blue-green solution. This precursor solution was added to 10 mL of aqueous solution of NH_2trz (0.1808 g, 2.15 mmol). A blue precipitate appeared after adding the first drops of the copper solution. The volume of distilled water was increased to 65 mL, and the solution was warmed at 80 °C for 3 h to dissolve the precipitate. A blue solution was obtained and kept for crystallization at room temperature. After 8 months, blue needle crystals were obtained. Yield: 0.1 g, 30%. IR (cm^{-1}): $\nu(NH_2)$ ~ 3230 (m), ν(N−N) ~ 1220 (m), ν(C−H out of plane) ~ 988 (m), ν(C−H ring torsion) = 625 (s), ν_1(Zr−F) ~ 590 (m).

$[Fe_3(NH_2trz)_{10}(H_2O)_2](SbF_6)_6 \cdot 1.5CH_3OH$ (12). $FeCl_2 \cdot 4H_2O$ (0.3 g, 1.51 mmol) and ~ 0.01 g of ascorbic acid dissolved in 5 mL of water were added to $KSbF_6$ (0.8294 g, 3.02 mmol) that was sparingly soluble in 10 mL of water. The resulting pale green solution of $[Fe(H_2O)_6](SbF_6)_2$ was added to a methanolic solution (5 mL) containing NH_2trz (0.3806 g, 4.5 mmol). An off white precipitate was formed after 10 min of continuous stirring at r.t. It was filtered, washed with 5−10 mL of methanol and dried in a desiccator. Yield: 0.8 g, 21%. Anal. for $Fe_3C_{21.5}H_{48}N_{40}O_{3.5}Sb_6F_{12}$ (2506.88 g/mol): calcd C, 10.30; H, 2.01; N, 22.35; Fe, 6.68. Found: C, 9.36; H, 2.64; N, 21.48; Fe, 6.5%. IR (cm^{-1}): $\nu(NH_2)$ ~3330 (s), ν(N−N) ~ 1221 (s), ν(C−H out of plane) ~ 997 (m), ν(C−H ring torsion) = 622 (s), ν(Sb−F) ~ 642, 732 (m).

$[Fe_3(NH_2trz)_{10}(H_2O)_2](SbF_6)_6 \cdot 0.5C_2H_5OH$ (13). It was synthesized following the same procedure as for **12** except that ethanol was used to dissolve NH_2trz. An off white precipitated was obtained. Yield: 1 g, 27%. Anal. for $Fe_3C_{21}H_{47}N_{40}O_{2.5}Sb_6F_{36}$ (2481.85 g/mol): calcd C, 10.18; H, 1.91; N, 22.62; Fe, 6.78. Found: C, 9,82; H, 2.60; N, 21.39; Fe, 6.58. IR (cm^{-1}): $\nu(NH_2)$ ~ 3300 (s), ν(N−N) ~ 1219, ν(C−H out of plane) ~ 1000, ν(C−H ring torsion) ~ 621(s), ν(Sb−F) ~ 745, 640 (m).

Physical Measurements. Elemental analyses were performed at University College London (U.K.). Atomic absorption analyses were carried out on a Perkin-Elmer 3110 spectrometer. Sampling was carried out in aqueous solutions containing nitric acid (65%). Standard solutions were prepared with Mohr's salt. IR spectra were collected on a BioRad FTS-135 spectrometer using KBr pellets and on a Shimadzu FTIR-84005. Thermogravimetric analyses (TGA) were performed in air (100 mL/min) at the heating rate of 1 °C/min from 293 to 400 K using a Mettler Toledo TGA/SDTA 851e analyzer. Diffuse reflectance spectra on solids were recorded with a CARY 5E spectrophotometer using polytetrafluoroethylene as a reference. Powder X-ray diffraction patterns were recorded on a Siemens D5000 counter diffractometer working with Cu Kα radiation and operating at room temperature. The samples were mounted on the support with silicon grease. ^{57}Fe Mössbauer spectra were recorded in transmission geometry over the temperature range (78−300 K) with conventional Mössbauer spectrometers equipped with a ^{57}Co(Rh) radioactive source operating at room temperature. The samples were sealed in aluminum foil and mounted on a nitrogen Oxford bath cryostat. The spectra were fitted to the sum of Lorentzians by a least-squares refinement using Mossfit[53] or Recoil 1.05 Mössbauer Analysis Software.[54] All isomer shifts refer to α-Fe at room temperature. Magnetic susceptibilities were measured in the temperature range 50−300 K using a MPMS-5 SQUID magnetometer. Data were corrected for magnetization of the sample holder and diamagnetic contributions, which were estimated from the Pascal constants. Differential scanning calorimetry measurements were carried out in a $He_{(g)}$ atmosphere using a Perkin-Elmer DSC Pyris 1 instrument equipped with a cryostat and operating down to 98 K. Aluminum capsules were loaded with 20−50 mg of sample and sealed. The heating and cooling rates were fixed at 5 and 10 K min^{-1}. Temperatures and enthalpies were calibrated over the temperature range of interest using the crystal−crystal transitions of pure cyclopentane (≥99%).[55] Diffuse reflectivity measurements were performed using a hydrostatic pressure device (operating with He gas) and an optical detection system which has been described in ref 46. The powder samples have been thermally cycled at least 10 times over the temperature range 78−300 K before starting the measurements. This thermal treatment led to the automilling of the crystallites because of the internal stress induced by the volume variation during the ST and ensures a full reproducibility of the hysteresis loop.[46] The light source used is a Quartz Tungsten Halogen lamp from LOT-ORIEL of 100 W maximal power, combined with an interferential filter operating at 550 nm. Scanning electron microscopy (SEM) was performed using a Gemini Digital Scanning Microscope 982 with 1 kV accelerating voltage with an aluminum sample holder.

Single Crystal X-ray Diffraction. The X-ray intensity data were collected at 100(1) K with a MAR345 image plate using Mo Kα (λ = 0.71069 Å) radiation. The crystal was mounted in an inert oil and transferred to the cold gas stream for flash cooling. The data were not corrected for absorption, but the data collection mode partially takes the absorption phenomena into account (78 images, $\Delta\Phi$ = 3, 15701 reflections measured for 3352 independent reflections). The crystal data and the data collection parameters are summarized in Table 1. The unit cell parameters were refined using all the collected spots after the integration process. The structure was solved by direct methods and refined by full-matrix least-squares on F^2 using SHELX97.[56] All the hydrogen atoms were localized by Fourier-difference synthesis. They were included in the refinement with a common isotropic temperature factor. The details of the refinement and

(53) Teillet, J.; Varret, F. *Mossfit*; unpublished work.
(54) Lagarec, K.; Rancourt, D. G. *Recoil, Mössbauer Spectral Analysis Software for Windows 1.0*; Department of Physics, University of Ottawa: Ottawa, Canada, 1998;
(55) Rotaru, A.; Dîrtu, M. M.; Enachescu, C.; Tanasa, R.; Linares, J.; Stancu, A.; Garcia, Y. *Polyhedron* **2009**, DOI: 10.1016/j.poly.2009.04.046.
(56) Sheldrick, G. M. *SHELX97, Program for crystal structure determination and refinement*; University of Göttingen: Göttingen, Germany, 1997.

the final *R* indices are presented in Table 1. CCDC 728233 for **11** contains the supplementary crystallographic data for this paper. These data can be obtained free of charge from the Cambridge Crystallographic Data Center via www.ccdc.cam.ac.uk/data_request/cif.

Acknowledgment. This work was partly funded by the IAP-VI (P6/17) INANOMAT programme, the FNRS (FRFC), the FSR de l'Université Catholique de Louvain, the Agence Universitaire de la Francophonie (ref. 63-13PS818) and the CNRS. M.M.D. acknowledges the Groupe Francophone de Spectromètrie Mössbauer (GFSM) for partially supporting her visit to ICAME 2007 (Kanpur, India). Dr A. Bhattacharjee and Prof. Dr. P. Gütlich are thanked for the SQUID measurement of (**8**).

Supporting Information Available: Overview of the Mössbauer parameters for **1**−**10** (Tables S1−S9) and selected Mössbauer spectra of **2**, **9**, **8** (Figure S1). This material is available free of charge via the Internet at http://pubs.acs.org.